molecular pharmaceutics

articles

Analysis of Amorphous Solid Dispersions Using 2D Solid-State NMR and ^{1}H T_1 Relaxation Measurements

Tran N. Pham,*,† Simon A. Watson,† Andrew J. Edwards,† Manisha Chavda,‡ Jacalyn S. Clawson,‡ Mark Strohmeier,‡ and Frederick G. Vogt*,‡

Chemical Development, GlaxoSmithKline plc, Gunnels Wood Road, Stevenage, Hertfordshire SG1 2NY, U.K., and Chemical Development, GlaxoSmithKline plc, 709 Swedeland Road, King of Prussia, Pennsylvania 19406

Received March 17, 2010; Accepted July 14, 2010

Abstract: Solid-state NMR (SSNMR) can provide detailed structural information about amorphous solid dispersions of pharmaceutical small molecules. In this study, the ability of SSNMR experiments based on dipolar correlation, spin diffusion, and relaxation measurements to characterize the structure of solid dispersions is explored. Observation of spin diffusion effects using the 2D ^{1}H−^{13}C cross-polarization heteronuclear correlation (CP-HETCOR) experiment is shown to be a useful probe of association between the amorphous drug and polymer that is capable of directly proving glass solution formation. Dispersions of acetaminophen and indomethacin in different polymers are examined using this approach, as well as ^{1}H double-quantum correlation experiments to probe additional structural features. ^{1}H−^{19}F CP-HETCOR serves a similar role for fluorinated drug molecules such as diflunisal in dispersions, providing a rapid means to prove the formation of a glass solution. Phase separation is detected using ^{13}C, ^{19}F, and ^{23}Na-detected ^{1}H T_1 experiments in crystalline and amorphous solid dispersions that contain small domains. ^{1}H T_1 measurements of amorphous nanosuspensions of trehalose and dextran illustrate the ability of SSNMR to detect domain size effects in dispersions that are not glass solutions via spin diffusion effects. Two previously unreported amorphous solid dispersions involving up to three components and containing voriconazole and telithromycin are analyzed using these experiments to demonstrate the general applicability of the approach.

Keywords: Amorphous solid dispersion; molecular dispersion; glass solution; nanosuspension; solid-state NMR; spin diffusion; heteronuclear correlation; double-quantum spectroscopy

Introduction

Developmental drug candidates have increasingly higher molecular weight and hydrophobicity, which lead to frequent instances of poor water solubility and low oral bioavailability.[1−3] The use of amorphous solid dispersions consisting of poorly water-soluble drugs and hydrophilic polymeric carriers can improve dissolution rate and oral bioavailability for many molecules, and can lead to successful marketed dosage forms.[4−9] In addition, amorphous solid dispersions play an important role in the early stage of development of poorly soluble drugs by maximizing exposure during animal ex-

* Corresponding authors. T.N.P.: GlaxoSmithKline plc, Gunnels Wood Road, Stevenage, Hertfordshire SG1 2NY, U.K.; e-mail, Tran.N.Pham@gsk.com. F.G.V.: GlaxoSmithKline plc, 709 Swedeland Road, King of Prussia, Pennsylvania 19406; Phone: 610 270 6895. Fax: 610 270 6727. E-mail, Fred.G.Vogt@gsk.com.

† GlaxoSmithKline plc, Gunnels Wood Road, Stevenage, Hertfordshire SG1 2NY, U.K.

‡ GlaxoSmithKline plc, 709 Swedeland Road, King of Prussia, PA.

(1) Lipinski, C. A. Drug-like properties and the causes of poor solubility and poor permeability. *J. Pharmacol. Toxicol. Methods* **2000**, *44*, 235–249.

(2) Streubel, A.; Siepmann, J.; Bodmeier, R. Drug delivery to the upper small intestine window using gastroretentive technologies. *Curr. Opin. Pharmacol.* **2006**, *6*, 501–508.

(3) Lobenberg, R.; Amidon, G. L. Modern bioavailability, bioequivalence and biopharmaceutics classification system. New scientific approaches to international regulatory standards. *Eur. J. Pharm. Biopharm.* **2000**, *50*, 3–12.

10.1021/mp100205g
Published on Web 07/14/2010

perimentation, allowing observation of toxicological effects and decreasing attrition in later stages of drug development.[10] Furthermore, solid dispersions of hydrophilic drugs and water-insoluble polymers can slow the dissolution rate of highly soluble drugs for use in controlled-release systems.[11,12] In solid dispersions, the pharmaceutical molecule can exist as a separated amorphous or crystalline phase, or may be present as an intimate mixture with the polymer where the degree of contact can vary from a molecular dispersion (i.e., a fully miscible solution, commonly referred to as a "glass solution") to phase-separated nano- or microdomains with amorphous or crystalline character.[5,13] The glass solution is often a desirable state for drug delivery, as it generally offers the benefits of high solubility with the least risk of phase separation and recrystallization into a less soluble crystalline state, while also potentially offering acceptable chemical stability.[5,13−15]

Amorphous dispersions are often characterized by differential scanning calorimetry (DSC) and other thermal methods, given the limited utility of conventional methods for characterizing crystalline materials like powder X-ray diffraction (PXRD).[5,13,16,17] Amorphous dispersions are normally characterized by PXRD methods simply to show the absence of any crystalline forms of the drug substance. DSC methods are commonly used to detect miscibility of the drug and polymer and formation of a glass solution via the observation of a single glass transition temperature (T_g) depressed from that in the pure polymer. DSC can also detect the appearance of multiple glass transition temperatures from the formation of an amorphous solid suspension, as with acetaminophen and piroxicam glass solutions,[18−21] and can also provide insight into drug−polymer miscibility and kinetic stabilization.[22] However, the complexity of dispersions leads to difficulties in applying thermal analysis as the sole characterization method.[23] Thermal methods provide fundamental information about the bulk properties of the material, but are limited in their structural information content and also can be difficult to interpret in cases where thermal events of interest are not well resolved. As a result, PXRD methods based on pair-distribution functions (PDF-PXRD) have recently been applied to the study of dispersions to supplement thermal analysis and provide additional structural information.[23,24] Infrared spectroscopy has also been widely employed to investigate structural effects in amorphous dispersions.[14,15,25] Transmission electron microscopy with ruthenium oxide staining has also been applied to spatially

(4) Serajuddin, A. T. M. Solid dispersion of poorly water-soluble drugs: Early promises, subsequent problems, and recent breakthroughs. *J. Pharm. Sci.* **1999**, *88*, 1058–1066.

(5) Janssens, S.; Van den Mooter, G. Physical chemistry of solid dispersions. *J. Pharm. Pharmacol.* **2009**, *61*, 1571–1586.

(6) Habib, M. J.; Venkataram, S.; Hussain, M. D. Fundamentals of solid dispersions. In *Pharmaceutical Solid Dispersion Technology*; Habib, M. J., Ed.; Technomic Publishing: Lancaster, PA, 2001; pp 7−35.

(7) Desai, J.; Alexander, K.; Riga, A. Characterization of polymeric dispersions of dimenhydrinate in ethyl cellulose for controlled release. *Int. J. Pharm.* **2006**, *308*, 115–123.

(8) Fawaz, F.; Bonini, F.; Guyot, M.; Bildet, J.; Maury, M.; Lagueny, A. M. Bioavailability of norfloxacin from PEG 6000 solid dispersion and cyclodextrin inclusion complexes in rabbits. *Int. J. Pharm.* **1996**, *132*, 271–275.

(9) Torrado, S.; Torrado, S.; Torrado, J. J.; Cadorniga, R. Preparation, dissolution and characterization of albendazole solid dispersions. *Int. J. Pharm.* **1996**, *140*, 247–250.

(10) Neervanna, S. Preclinical formulations for discovery and toxicology: Physicochemical challenges. *Expert Opin. Drug Metab. Toxicol.* **2006**, *2*, 715–731.

(11) Pignatello, R.; Bucolo, C.; Ferrara, P.; Maltese, A.; Puleo, A.; Puglisi, G. Eudragit RS100® nanosuspensions for the ophthalmic controlled delivery of ibuprofen. *Eur. J. Pharm. Sci.* **2002**, *16*, 53–61.

(12) Pignatello, R.; Ferro, M.; De Guidi, G.; Salemi, G.; Vandelli, M. A.; Guccione, S.; Geppi, M.; Forte, C.; Puglisi, G. Preparation, characterization and photosensitivity studies of solid dispersions of diflunisal and Eudragit RS100® and RL100®. *Int. J. Pharm.* **2001**, *218*, 27–42.

(13) Chiou, W. L.; Riegelman, S. Pharmaceutical applications of solid dispersion systems. *J. Pharm. Sci.* **1971**, *60*, 1281–1302.

(14) Rumondor, A. C. F.; Marsac, P. J.; Stanford, L. A.; Taylor, L. S. Phase behavior of poly(vinylpyrrolidone) containing amorphous solid dispersions in the presence of moisture. *Mol. Pharmaceutics* **2009**, *6*, 1492–1505.

(15) Rumondor, A. C. F.; Taylor, L. S. Effect of polymer hygroscopicity on the phase behavior of amorphous solid dispersions in the presence of moisture. *Mol. Pharmaceutics* **2010**, *7*, 477–490.

(16) Byrn, S. R. Pfeiffer, R. R. Stowell, J. G. *Solid-state Chemistry of Drugs*; SSCI: West Lafayette, IN, 1999.

(17) Bernstein, J. *Polymorphism in Molecular Crystals.*: Oxford University Press: New York, 2002.

(18) Ozeki, T.; Hiroshi, Y.; Kanaya, Y. Application of the solid dispersion method to the controlled release of medicine. IX. Difference in the release of flurbiprofen from solid dispersions with poly(ethylene oxide) and hydroxypropylcellulose and the interaction between medicine and polymers. *Int. J. Pharm.* **1997**, *155*, 209–217.

(19) Jachowicz, R.; Nurnberg, E.; Pieszczek, B.; Kluczykowska, B.; Maciejewska, A. Solid dispersion of ketoprofen in pellets. *Int. J. Pharm.* **2000**, *206*, 13–21.

(20) de Villiers, M. M.; Wurster, D. E.; Van der Watt, J. G.; Ketkar, A. X-Ray powder diffraction determination of the relative amount of crystalline acetaminophen in solid dispersions with polyvinylpyrrolidone. *Int. J. Pharm.* **1998**, *163*, 219–224.

(21) Tantishaiyakul, V.; Kaewnopparat, N.; Ingkatawornwong, S. Properties of solid dispersions of piroxicam in polyvinylpyrrolidone K-30. *Int. J. Pharm.* **1996**, *143*, 59–66.

(22) Paudel, A.; Van Humbeeck, J.; Van den Mooter, G. Theoretical and experimental investigation on the solid solubility and miscibility of naproxen in polyvinylpyrrolidone. *Mol. Pharmaceutics* [Online early access]. DOI: 10.1021/mp100013p. Published online: June 21, 2010.

(23) Newman, A.; Engers, D.; Bates, S.; Ivanisevic, I.; Kelly, R. C.; Zografi, G. Characterization of amorphous API:polymer mixtures using X-ray powder diffraction. *J. Pharm. Sci.* **2008**, *97*, 4840–4857.

(24) Ivanisevic, I.; Bates, S.; Chen, P. Novel methods for the assessment of miscibility of amorphous drug-polymer dispersions. *J. Pharm. Sci.* **2009**, *98*, 3373–3386.

(25) Taylor, L. S.; Zografi, G. Spectroscopic characterization of interactions between PVP and indomethacin as amorphous molecular dispersions. *Pharm. Res.* **1997**, *14*, 1691–1698.

distinguish between amorphous and crystalline phases in related systems.[26]

Solid-state NMR (SSNMR) is also a useful method for the characterization of amorphous dispersions, because it allows access to detailed information on molecular structure, dynamics, and domain morphology in small molecule and macromolecular systems.[27] For example, ^{13}C SSNMR methods have been applied to ibuprofen and flurbiprofen in Eudragit RL100 dispersions,[28,29] ketoprofen in poly(ethylene oxide),[31] and indomethacin in cyclodextrin.[32] SSNMR has been used to establish a correlation between the ^{13}C line width of indomethacin and its apparent equilibrium solubility in silica and polyvinylpyrrolidone (PVP), enabling prediction of the drug solubility in the carrier.[33,34] Multivariate analysis of ^{13}C SSNMR spectra of troglitazone/PVP dispersions allowed prediction of recrystallization behavior of the drug.[35] However, detailed structural analyses of amorphous dispersions using recently developed 2D SSNMR experiments and observation of high-resolution ^{1}H spectra (either directly or indirectly) have been restricted to several examples focused on the molecular conformation of the drug or on hydrogen bonding.[28−30] More extensive use of 2D SSNMR dipolar correlation methods can directly probe interactions between amorphous materials and small molecules by measuring direct dipolar interactions, spin diffusion, and ^{1}H spin−lattice (T_1) relaxation times. Spin diffusion effects are particularly useful as they can be exploited in SSNMR experiments during periods where magnetization is spin-locked or stored longitudinally, and can cover a range from tens of angstroms to hundreds of nanometers.[36,37] For example, $^{1}H-^{1}H$ 2D spin diffusion experiments at a high magnetic field can detect interactions between nanoparticles of probucol, an enteric methacrylic acid−methyl methacrylate polymer, and a surfactant.[38] Several features of amorphous dispersions make them suitable for ^{1}H spin diffusion studies. The functional groups in polymers used to form amorphous dispersions via spray-drying and hot-melt extrusion are generally confined to aliphatic proton environments. This allows for the detection of ^{1}H spin diffusion to aromatic protons commonly found in drugs by dipolar correlation via heteronuclear correlation (HETCOR) experiments. Most of the popular polymers used in dispersions are amenable to these methods, including PVP, PVP vinyl acetate copolymers (PVP-VA), polyethylene glycol (PEG), hydroxypropylmethylcellulose (HPMC), HPMC substituted with acetate and succinate groups (HPMC-AS), and caprolactam-based polymers.[39] Only less-commonly encountered polymers such as hypromellose phthalate contain potentially interfering aromatic groups. The distances of interest between the drug and polymer are particularly amendable to spin diffusion analysis, as they can range from 5−10 Å in the case of glass solutions to >100 Å in the case of suspensions and can be detected via spectral features (such as 2D correlations) if within range.

In the present work, we describe 2D SSNMR approaches to the analysis of the structure of amorphous dispersions, with a particular focus on novel methods for proving the presence of the desirable glass solution via 2D methods. This is accomplished using direct dipolar coupling, spin diffusion, and relaxation methods, which can be detected via high-resolution experiments correlating $^{1}H-^{1}H$, $^{1}H-^{13}C$, $^{1}H-^{19}F$, and other nuclei. The approach used here examines the local molecular environment of the drug molecule, the association and interactions between the drug and the polymer, and longer range effects including the appearance of nano- and microsuspensions within the polymer. A similar SSNMR approach was used to study molecular association and

(26) Trent, J. S.; Scheinbeim, J. I.; Couchman, P. R. Ruthenium tetraoxide staining of polymers for electron microscopy. *Macromolecules* **1983**, *16*, 589–598.
(27) Schmidt-Rohr, K.; Spiess, H. W. *Multidimentional Solid-State NMR and Polymers*: Academic Press: London, 1994.
(28) Geppi, M.; Guccione, S. Molecular properties of ibuprofen and its solid dispersions with Eudragit RL100 studied by solid-state nuclear magnetic resonance. *Pharm. Res.* **2005**, *22*, 1544–1555.
(29) Mollica, G.; Geppi, M.; Pignatello, R.; Veracini, C. A. Molecular properties of flurbiprofen and its solid dispersions with Eudragit RL100 studied by high- and low-resolution solid-state nuclear magnetic resonance. *Pharm. Res.* **2006**, *23*, 2129–2140.
(30) Tobyn, M.; Brown, J.; Dennis, A. B.; Fakes, M.; Gao, Q.; Gamble, J.; Khimyak, Y. Z.; McGeorge, G.; Patel, C.; Sinclair, W.; Timmins, P.; Yin, S. Amorphous drug-PVP dispersions: Application of theoretical, thermal and spectroscopic analytical techniques to the study of a molecule with intermolecular bonds in both the crystalline and pure amorphous state. *J. Pharm. Sci.* **2009**, *98*, 3456–3468.
(31) Schachter, D. M.; Xiong, J.; Tirol, G. C. Solid state NMR perspective of drug-polymer solid solutions: a model system based on poly(ethylene oxide). *Int. J. Pharm.* **2004**, *281*, 89–101.
(32) Wulff, M.; Alden, M.; Tegenfeldt, J. Solid-state NMR investigation of indomethacin-cyclodextrin complexes in PEG 6000 carrier. *Bioconjugate Chem.* **2002**, *13*, 240–248.
(33) Watanabe, T.; Hasegawa, S.; Wakiyama, N.; Kusai, A.; Senna, M. Prediction of apparent equilibrium solubility of indomethacin compounded with silica by ^{13}C solid state NMR. *Int. J. Pharm.* **2002**, *248*, 123–129.
(34) Watanabe, T.; Hasegawa, S.; Wakiyama, N.; Kusai, A.; Senna, M. Comparision between polyvinylpyrrolidone and silica nanoparticles as carriers for indomethacin in a solid state dispersion. *Int. J. Pharm.* **2003**, *250*, 283–286.
(35) Ito, A.; Watanabe, T.; Yada, S.; Hamaura, T.; Nakagami, H.; Higashi, K.; Moribe, K.; Yamamoto, K. Prediction of recrystallization behavior of troglitazone/polyvinylpyrrolidone solid dispersion by solid-state NMR. *Int. J. Pharm.* **2010**, *383*, 18–23.
(36) Meier, B. H. Polarization transfer and spin diffusion in solid-state NMR. *Adv. Magn. Opt. Reson.* **1994**, *18*, 1–116.
(37) Cheung, T. T. P. Spin diffusion in solids. In *The Encyclopedia of NMR*; Harris, R. K., Grant, D. M., Eds.; Wiley: New York, 1996; pp 4518−4524.
(38) Io, T.; Fukami, T.; Yamamoto, K.; Suzuki, T.; Xu, J.; Tomono, K.; Ramamoorthy, A. Homogeneous nanoparticles to enhance the efficiency of a hydrophobic drug, antihyperlipidemic probucol, characterized by solid-state NMR. *Mol. Pharmaceutics* **2010**, *7*, 299–305.
(39) Owusu-Ababio, G. Use of polymers in solid dispersion technology. In *Pharmaceutical Solid Dispersion Technology*; Habib, M. J., Ed.; Technomic Publishing: Lancaster, PA, 2001; pp 65−86.

structure in cocrystals and crystalline solid solutions.[40,41] Samples in the present work have been prepared by solvent evaporation or lyophilization, common screening approaches used for dispersions before scale-up spray-drying and hot-melt extrusion approaches are applied, to highlight the capability of SSNMR to answer structural questions on initial preparations with small amounts of material.[4−6] The use of SSNMR to study molecular mobility is not treated in the present work, although this is an important complementary use of the technique,[42−45] as mobility can often be related to chemical or physical stability of the drug in an amorphous dispersion.

Experimental Section

Solid Dispersions. Dispersions of acetaminophen in PVP were prepared by rapid solvent evaporation from ethanol solutions under reduced pressure.[20] Acetaminophen was obtained from Sigma-Aldrich (St. Louis, MO). PVP Kollidon 30 (K30 grade, with an average molecular weight of 30−40 kDa) was obtained from BASF (Ludwigshafen, Germany) and Acros (Geel, Belgium). Both materials were used as received. Samples containing 30% and 70% w/w acetaminophen were prepared by dissolving approximately 1 g total mass in 20 mL of ethanol and vacuum-drying at 50 °C for 2 days to obtain white to off-white solids, which were pulverized using a mortar and pestle. Additional samples with 30% w/w acetaminophen were similarly prepared using an ammonio methacrylate copolymer (Eudragit RS PO) and a butyl methacrylate−(2-dimethylaminoethyl) methacrylate−methyl methacrylate copolymer (Eudragit E PO) obtained from Degussa (Darmstadt, Germany), and hydroxypropylcellulose (HPC) obtained from Nisso (New York, NY). Amorphous acetaminophen was prepared by melting 30 mg of crystalline material at 200 °C and quenching in liquid N_2.

Dispersions of indomethacin were prepared by rapid evaporation from dichloromethane solution under 25 in. Hg vacuum at 50 °C.[23] Indomethacin was obtained from Sigma-Aldrich and used as received. Approximately 300 mg of indomethacin and 700 mg of PVP K30 were combined in 60 mL of CH_2Cl_2 and vacuum-dried at 50 °C for 2 days. Yellow solids were obtained as previously described;[23,25] these were collected by scraping for analysis. A deuterium-exchanged dispersion was obtained by exchanging the above sample in a 75% RH D_2O chamber (prepared using saturated NaCl in D_2O) for 2 weeks, followed by vacuum drying for 1 h. The vacuum drying step was necessary to remove a large liquid water peak from the ^2H SSNMR spectrum. The sample was analyzed immediately after removal from the nitrogen-purged vacuum oven to avoid back-exchange with atmospheric H_2O. Amorphous indomethacin was prepared by melting 30 mg of crystalline material at approximately 180 °C and quenching in liquid N_2. The solids were then scraped and physically mixed with 70 mg of PVP K30 in a small vial to create a 30% w/w physical mixture.

Dextran (M_n 64−76 kDa) and D-(+)-trehalose dihydrate were obtained from Sigma-Aldrich and Avocado/Alfa Aesar (Ward Hill, MA), respectively. Trehalose-dextran amorphous dispersions containing 30% and 50% w/w trehalose were prepared by overnight freeze-drying from ∼10% w/w aqueous solutions using a Heto Drywinner lyophilizer model CT/DW 110.

Dispersions of diflunisal in PVP K30 were prepared by rapid evaporation from ethanol.[46] Approximately 300 mg of diflunisal (Sigma-Aldrich), used as received, and 700 mg of PVP K30 were evaporated from 30 mL of ethanol under 25 in. Hg vacuum at 50 °C for 5 days. A second sample was prepared using 750 mg of diflunisal and 250 mg of PVP in the same manner.

A dispersion of telithromycin in PVP K30 was prepared by evaporation of 300 mg of telithromycin and 700 mg of PVP from 15 mL of CH_2Cl_2. Telithromycin was obtained from AK Scientific (Mountain View, CA) and used as received. Finally, a ternary dispersion of voriconazole, PVP K30, and sodium lauryl sulfate (SLS) was prepared by rapid evaporation from a 30 mL ethanol solution using 150 mg of voriconazole, 50 mg of SLS, and 800 mg of PVP K30 after sonication. Voriconazole was obtained from AK Scientific and used as received. SLS was purchased from Sigma-Aldrich and used as received.

SSNMR Spectroscopy. SSNMR experiments were performed using Bruker Avance 360, Avance 400 and Avance II+ 500 triple-resonance spectrometers operating at ^1H frequencies of 360.13, 399.87, and 500.13 MHz, respectively. Experiments were performed at 273 K unless otherwise noted. ^1H SSNMR experiments were performed using Bruker 2.5 mm double- and triple-resonance magic-angle spinning (MAS) probes spinning

(40) Vogt, F. G.; Clawson, J. S.; Strohmeier, M.; Edwards, A. J.; Pham, T. N.; Watson, S. A. Solid-state NMR analysis of organic cocrystals and complexes. *Cryst. Growth Des.* **2009**, *9*, 921–937.

(41) Vogt, F. G.; Vena, J. A.; Chavda, M.; Clawson, J. S.; Strohmeier, M.; Barnett, M. E. Structural analysis of 5-fluorouracil and thymine solid solutions. *J. Mol. Struct.* **2009**, *932*, 16–30.

(42) Lubach, J. W.; Xu, D.; Segmuller, B. E.; Munson, E. J. Investigation of the effects of pharmaceutical processing upon solid-state NMR relaxation times and implications to solid-state formulation stability. *J. Pharm. Sci.* **2007**, *96*, 777–787.

(43) Aso, Y.; Yoshioka, S.; Kojima, S. Relationship between the crystallization rates of amorphous nifedipine, phenobarbital, and flopropione, and their molecular mobility as measured by their enthalpy relaxation and ^1H NMR relaxation times. *J. Pharm. Sci.* **2000**, *89*, 408–416.

(44) Forster, A.; Apperly, D.; Hempenstall, J.; Lancaster, R.; Rades, T. Investigation of the physical stability of amorphous drug and drug/polymer melts using variable temperature solid state NMR. *Pharmazie* **2003**, *58*, 761–762.

(45) Aso, Y.; Yoshioka, S.; Miyazaki, T.; Kawanishi, T. Feasibility of ^{19}F-NMR for assessing the molecular mobility of flufenamic acid in solid dispersions. *Chem. Pharm. Bull.* **2009**, *57*, 61–64.

(46) Martinez-Oharriz, M. C.; Rodriguez-Espinosa, C.; Martin, C.; Goni, M. M.; Tros-Ilarduya, M. C.; Sanchez, M. Solid dispersions of diflunisal-PVP: Polymorphic and amorphous states of the drug. *Drug Dev. Ind. Pharm.* **2002**, *28*, 717–725.

at a rate (υ_r) of 35 kHz. ^{1}H direct-polarization MAS (DP-MAS) experiments used a 2.5 μs excitation pulse, 60 s relaxation delays, and between 16 and 64 acquired transients. ^{13}C and ^{19}F SSNMR spectra were obtained with Bruker 4 mm triple resonance HFX MAS probes tuned to ^{1}H, ^{19}F, and ^{13}C frequencies or HXY MAS probes in double-resonance mode and tuned to ^{1}H and ^{13}C frequencies. Cross-polarization (CP) transfers were performed at power levels of 55−80 kHz; the power level was ramped linearly during the contact time over a depth of 15 to 20 kHz on the ^{1}H channel to enhance CP efficiency.[47] ^{13}C CP spectra were obtained at $\upsilon_r = 8$ kHz with a five-pulse total sideband suppression (CP-TOSS) sequence.[48] ^{1}H heteronuclear decoupling was performed at an RF power of 105 kHz using the SPINAL-64 pulse sequence, and ^{19}F decoupling made use of a series of π pulses (one per rotor period).[49,50] Edited ^{13}C spectra containing only quaternary and methyl signals were obtained using dipolar dephasing (also known as nonquaternary suppression or NQS) during the TOSS period and three subsequent rotor periods using a shifted echo pulse sequence.[48,51] ^{2}H DP-MAS experiments were performed using a 4 mm HFX probe with a single 3.5 μs excitation pulse and a 5 s relaxation delay. ^{13}C spectra were referenced to tetramethylsilane (TMS) using an external reference sample of hexamethylbenzene.[52] ^{19}F spectra were also obtained using both CP-MAS and DP-MAS methods. ^{19}F spectra were referenced to $CFCl_3$ via calculation from the experimental ^{13}C references with the unified scale method.[53] ^{1}H spectra were referenced via the unified scale method and checked by addition of a small amount of liquid TMS to samples. ^{23}Na spectra were obtained using both 4 mm and 2.5 mm MAS probes referenced to solid NaCl at 0 ppm. ^{2}H spectra were externally referenced using a sample of d_4-malonic acid relative to an average value of 3.3 ppm for the methylene protons;[54] this sample was also used to verify the accurate setting of the magic angle for ^{2}H MAS experiments.[55]

Proton spin−lattice relaxation times (^{1}H T_1) were determined via ^{1}H, ^{13}C, ^{23}Na, and ^{19}F-detection using saturation recovery with a 100-pulse saturation comb; when ^{13}C-detection was utilized, a five-pulse CP-TOSS period was added to the end of the experiment. This pulse sequence obtains similar results to heteronuclear-detected ^{1}H T_1 experiments that have been previously reported,[56] but offers advantages in speed and sideband suppression for dealing with more complex pharmaceutical systems. Samples were spun or purged for at least two days using N_2 gas to avoid changes in ^{1}H T_1 relaxation times measured at different points caused by the absence of oxygen; polymers are particularly sensitive to these effects because of their permeability to oxygen gas. For analysis of ^{1}H T_1 data, spectral deconvolution was employed in order to obtain more accurate integrals of overlapped peaks using the DMfit software package,[57] and least-squares fitting and estimation of error was performed using standard methods.[58]

Several more advanced 2D SSNMR experiments were applied in this work as discussed in detail in the following sections. Experimental details for these experiments are given here. 2D rotor-synchronized ^{1}H double-quantum broadband back-to-back (DQ-BABA) MAS experiments were performed with 2.5 mm probes at $\upsilon_r = 35$ kHz using two rotor periods of double-quantum excitation and two rotor periods of reconversion.[59] 2D CP heteronuclear correlation (CP-HETCOR) experiments between ^{1}H and ^{13}C, ^{19}F, and ^{23}Na nuclei were obtained using 4 mm probes with υ_r set between 12.5 and 15 kHz and frequency-switched Lee−Goldburg (FSLG) homonuclear decoupling at 105 kHz.[60] Ramp CP transfers were used for HETCOR experiments with durations ranging from 500 μs to 2 ms. Lee−Goldburg CP (LGCP) transfers were matched to the −1 Hartman−Hahn sideband.[61] When FSLG was used for homonuclear decoupling, the

(47) Metz, G.; Wu, X.; Smith, S. O. Ramped-amplitude cross-polarization in magic-angle spinning NMR. *J. Magn. Reson. A* **1994**, *110*, 219–227.

(48) Antzutkin, O. N. Sideband manipulation in magic-angle spinning NMR. *Prog. Nucl. Magn. Reson. Spectrosc.* **1999**, *35*, 203–266.

(49) Fung, B. M.; Khitrin, A. K.; Ermolaev, K. An improved broadband decoupling sequence for liquid crystals and powders. *J. Magn. Reson.* **2000**, *142*, 97–101.

(50) Hodgkinson, P. Heteronuclear decoupling in the NMR of solids. *Prog. Nucl. Magn. Reson. Spectrosc.* **2005**, *46*, 197–222.

(51) Opella, S. J.; Frey, M. H. Selection of non-protonated carbon resonances in solid-state NMR. *J. Am. Chem. Soc.* **1979**, *101*, 5854–5856.

(52) Earl, W. L.; Vanderhart, D. L. Measurement of ^{13}C chemical shifts in solids. *J. Magn. Reson.* **1982**, *48*, 35–54.

(53) Harris, R. K.; Becker, E. D.; Cabral de Menezes, S. M.; Goodfellow, R.; Granger, P. NMR nomenclature. Nuclear spin properties and conventions for chemical shifts (IUPAC recommendations 2001). *Pure Appl. Chem.* **2001**, *73*, 1795–1818.

(54) Sagnowski, S. F.; Aravamudhan, S.; Haeberlen, U. Wide-line and high-resolution proton magnetic resonance in single crystals of malonic acid. *J. Magn. Reson.* **1977**, *28*, 271–288.

(55) Kristensen, J. H.; Bildsøe, H.; Jakobsen, H. J.; Nielsen, N. C. Deuterium quadrupole couplings from least-squares computer simulations of ^{2}H MAS NMR spectra. *J. Magn. Reson.* **1991**, *92*, 443–453.

(56) Zumbulyadis, N.; Antalek, B.; Windig, W.; Scaringe, R. P.; Lanzafame, A. M.; Blanton, T.; Helber, M. Elucidation of polymorph mixtures using solid-state ^{13}C CP/MAS NMR spectroscopy and direct exponential curve resolution algorithm. *J. Am. Chem. Soc.* **1999**, *121*, 11554–11557.

(57) Massiot, D.; Fayon, F.; Capron, M.; King, I.; Le Calve, S.; Alonso, B.; Durand, J. O.; Bujoli, B.; Gan, Z.; Hoatson, G. Modelling one- and two-dimensional solid-state NMR spectra. *Magn. Reson. Chem.* **2002**, *40*, 70–76.

(58) Bevington, P. R.; Robinson, D. K. *Data reduction and error analysis for the physical sciences*, 3rd ed.; McGraw-Hill: New York, 2003; pp 142−163.

(59) Feike, M.; Demco, D. E.; Graf, R.; Gottwald, J.; Hafner, S.; Spiess, H. W. Broadband multiple-quantum NMR spectroscopy. *J. Magn. Reson. A* **1996**, *122*, 214–221.

(60) van Rossum, B. J.; Förster, H.; de Groot, H. J. M. High-field and high-speed CP-MAS ^{13}C NMR heteronuclear dipolar-correlation spectroscopy of solids with frequency-switched Lee-Goldburg homonuclear decoupling. *J. Magn. Reson.* **1997**, *124*, 516–519.

(61) van Rossum, B. J.; de Groot, C. P.; Ladizhansky, V.; Vega, S.; de Groot, H. J. M. A method for measuring heteronuclear (^{1}H-^{13}C) distances in high speed MAS NMR. *J. Am. Chem. Soc.* **2000**, *122*, 3465–3472.

sample was restricted to the center of the 4 mm rotors to maximize RF homogeneity. The HETCOR experiments were performed so that the entire spectrum was recorded with $F_1 > 0$ Hz (where F_1 is the indirectly detected ^{1}H frequency dimension and F_2 is the directly detected dimension) to avoid quadrature images and artifacts at 0 Hz in the ^{1}H spectrum ($F_1 = 0$ Hz) that are common to this experiment; artifacts at $F_1 = 0$ Hz were also zeroed out after processing. The ^{19}F CP-DARR experiment was performed at $\upsilon_r = 15$ kHz using mixing periods given in the text.[62] ^{23}Na multiple-quantum MAS (MQ-MAS) experiments were performed at 11.7 T and $\upsilon_r = 25$ kHz using a 2.5 mm Bruker HFX probe and a three-pulse triple-quantum z-filtered experiment, with a shearing transformation applied.[63,64] The experiments used a 4 μs excitation pulse and a 1.6 μs reconversion pulse with an RF power of ~150 kHz, and a 16 μs z-filter pulse with an RF power of ~40 kHz.

Powder X-ray Diffraction and Differential Scanning Calorimetry. PXRD patterns were obtained using a Panalytical X'Pert Pro diffractometer equipped with an X'Celerator Real Time Multi-Strip (RTMS) detector. Samples were flattened onto a zero-background silicon holder and run immediately after preparation. A continuous 2θ scan range of 2° to 40° was used with a Cu Kα (1.5418 Å) radiation source and a generator power of 40 kV and 40 mA. A step size of 0.0167 degrees per 2θ step was used, and individual patterns required 5 min to obtain. Samples were analyzed at ambient temperature and humidity and were rotated at 25 rpm. Modulated DSC (mDSC) was performed using a TA Instruments Q2000 system with a heating rate of 1 °C/min.

Results and Discussion

Acetaminophen Dispersions. Dispersions of acetaminophen in PVP provide a simple starting point to illustrate the capabilities of the SSNMR methods used to characterize dispersions. This system has been extensively studied by other physical methods, and is known to be a glass solution at low drug concentrations that phase separates into crystalline form I as the drug concentration increases.[20] The crystalline acetaminophen used in this study was obtained as the monoclinic phase-pure form I, as confirmed by PXRD analysis and comparison to a simulated PXRD pattern (CSD refcode HXACAN01, see Supporting Information).[65−67] ^{13}C CP-TOSS spectra of PVP dispersions containing 30% and 70% w/w acetaminophen are shown in Figure 1. The spectra are assigned in reference to the numbered structures of acetaminophen (**I**) and PVP (**II**). The numbering scheme used for acetaminophen is taken from the crystal structure.[65] The assignments shown for the spectra of **I** and **II** are based on chemical shift trends and previously reported values.[66] The ^{13}C CP-TOSS spectrum of the 30% w/w dispersion shows broad peaks indicative of amorphous material (Figure 1). In the spectrum of the 70% w/w acetaminophen dispersion, both crystalline form I and amorphous material are observed. No changes to the spectrum of the 30% w/w or 70% w/w sample were observed after one year of storage at ambient conditions, apart from the signal at 57.9 ppm, which is indicative of a small amount of ethanol bound to PVP and was seen to disappear after storage for one year.

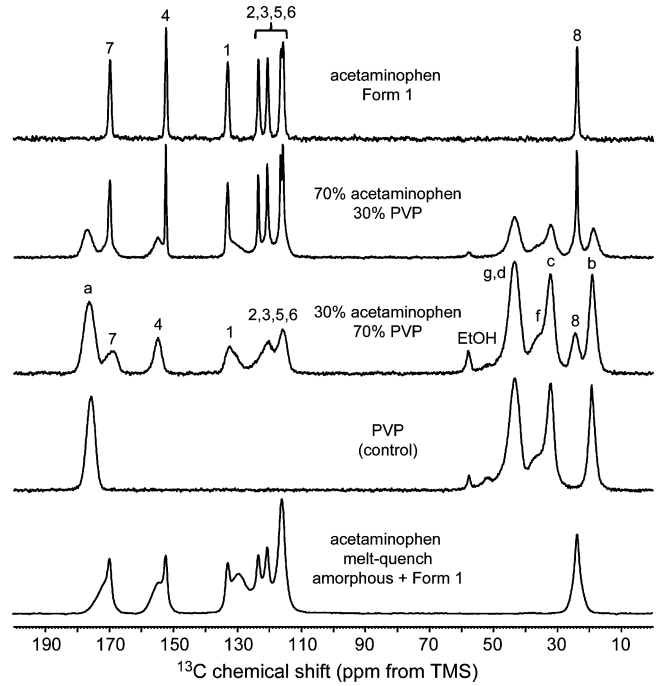

Figure 1. ^{13}C CP-TOSS spectra ($\upsilon_r = 8$ kHz) of dispersions of acetaminophen in PVP, compared with the spectrum of crystalline acetaminophen form I (**I**) and PVP. Assignments are shown in reference to schemes **I** and **II**. Spectra were obtained at 9.4 T and 273 K.

The results of ^{1}H MAS experiments on the 30% dispersion of **I** are shown in Figure 2. The ^{1}H MAS spectrum of the dispersion is compared with a spectrum of crystalline form I and PVP. A deshielded signal in the spectrum of the dispersion is seen at 10.4 ppm, similar to a peak observed form I, and is assigned to the amide N1(H) and O1(H5) protons (the latter assignment is confirmed by a C4−O1(H5) correlation in the ^{1}H−^{13}C CP-HETCOR spectrum discussed below). This indicates that, in the 30% w/w amorphous dispersion of **I**, the OH group is likely engaged in a hydrogen bond, as was also observed using ^{1}H MAS NMR for another

(62) Takegoshi, K.; Nakamura, S.; Terao, T. ^{13}C-^{1}H dipolar-driven ^{13}C-^{13}C recoupling without ^{13}C RF irradiation in nuclear magnetic resonance of rotating solids. *J. Chem. Phys.* **2003**, *118*, 2325–2341.

(63) Amoureux, J.-P.; Fernandez, C.; Steuernagel, S. Z filtering in MQMAS NMR. *J. Magn. Reson. A* **1996**, *123*, 116–118.

(64) Rocha, J.; Morais, C. M.; Fernandez, C. Progress in multiple-quantum magic-angle-spinning NMR spectroscopy. *Top. Cur. Chem.* **2005**, *246*, 141–194.

(65) Haisa, M.; Kashino, S.; Kawai, R.; Maeda, H. The monoclinic form of p-hydroxyacetanilide. *Acta Crystallogr.* **1976**, *B32*, 1283–1285.

(66) Moynihan, H. A.; O'Hare, I. P. Spectroscopic characterization of the monoclinic and orthorhombic forms of paracetamol. *Int. J. Pharm.* **2002**, *247*, 179–185.

(67) Nichols, G.; Frampton, C. S. Physicochemical characterization of the orthorhombic polymorph of paracetamol crystallized from solution. *J. Pharm. Sci.* **1998**, *87*, 684–693.

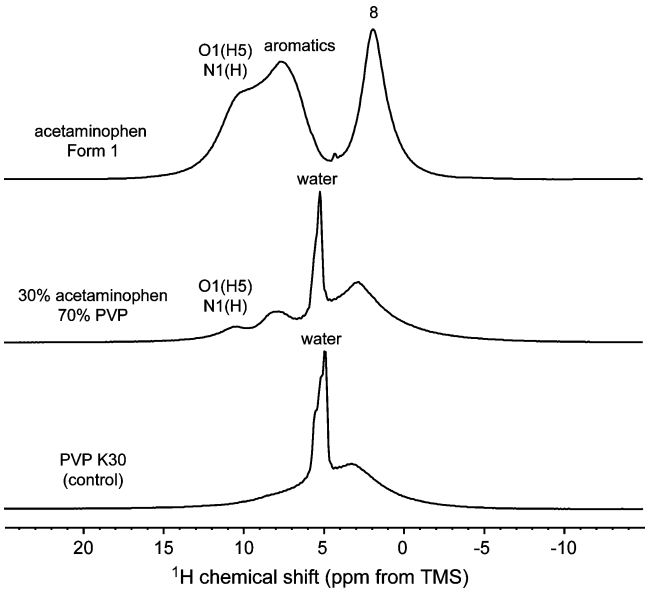

Figure 2. ¹H MAS spectrum (υ_r = 35 kHz) of the 30% w/w amorphous dispersion of acetaminophen (**I**) in PVP (**II**), compared with the spectra of crystalline **I** (form I) and PVP. Spectra were obtained at 9.4 T and 273 K.

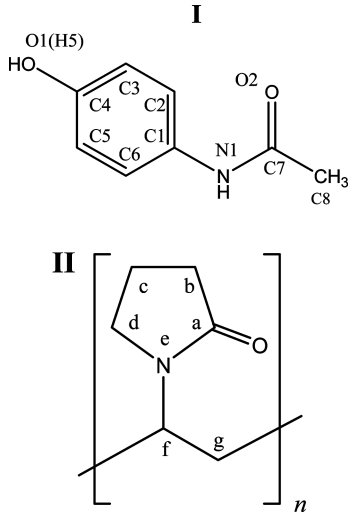

drug−polymer dispersion.[30] The O−H···O hydrogen-bond distance in the dispersion can be estimated since the H···O distance r_{OH} is known to be linearly dependent on the ¹H isotropic chemical shift δ from assembled crystallographic and NMR data through the equation[68]

$$r_{OH} = (2.210 \pm 0.005) - (0.044 \pm 0.004)\delta \qquad (1)$$

The O−H···O distance predicted for the dispersion from the ¹H chemical shift is therefore 1.75 ± 0.04 Å, and likely involves the PVP carbonyl group as the acceptor; this distance is typical for organic crystals and is similar to that found in the neutron diffraction structure of form I.[30,69]

In Figure 3(a), ¹H−¹³C CP-HETCOR spectra are shown for the 30% w/w dispersion of **I**, obtained at two different contact times of 0.5 and 1 ms. The arrows denote correlations between ¹³C PVP signals and protons in the aromatic and phenolic region (8−10 ppm) that directly illustrate molecular association between PVP and **I**. As the contact time increases, direct dipolar couplings are increasingly supplemented by ¹H−¹H spin diffusion effects during the CP spin-lock period, leading to short-range effects that are ultimately limited by spin−lattice relaxation in the rotating frame (¹H $T_{1\rho}$). These effects can be seen in the extracted rows shown in Figure 3(b), where the increase in contact time from 0.5 to 1 ms leads to a relative increase in the PVP signal intensity (marked by arrows) in the row at F_1 = 8.1 ppm. The range of ¹H−¹H spin diffusion effects can be estimated from the maximum diffusion path length (L) during a 1 ms contact time period, which is related to the spin diffusion coefficient (D) and the time (t) over which the spin diffusion takes place (e.g., the contact time) by[70−72]

$$\langle L^2 \rangle = 6Dt \qquad (2)$$

where the brackets denote an ensemble average. The spin diffusion coefficient in eq 2 may be estimated as $D = \langle l_0^2 \rangle / T_2$, where l_0 is the distance between protons, estimated as 0.1 nm, and T_2 is the spin−spin relaxation time, estimated at 100 μs.[70,71] For a 500 μs contact time, eq 2 yields an average L of about 5 Å as a maximum range over which ¹H−¹H spin diffusion can occur within the ¹H spin-lock during the contact time of a CP-HETCOR experiment. In the experiments used in the remainder of this work, the contact times do not exceed 2 ms, yielding a range of about 11 Å. In addition, the direct dipolar ¹H−X interaction that is transferred by the CP-HETCOR experiment is limited in range to 3−5 Å given the r^{-3} dependence of the dipolar coupling (where r is the internuclear distance).[60,61] Finally, a large percentage of the molecules must be in intimate contact to produce signals in these experiments; thus domains of >100 Å are unlikely to give rise to any correlations because only a tiny percentage of molecules at the surfaces of the domains would be in contact. For these reasons, the ¹H−X CP-HETCOR spectrum provides definitive evidence of mo-

(68) Zhou, D. H.; Rienstra, C. M. Rapid analysis of organic compounds by proton-detected heteronuclear correlation NMR spectroscopy with 40 kHz magic-angle spinning. *Angew. Chem., Int. Ed.* **2008**, *47*, 7328–7331.

(69) Wilson, C. C.; Shankland, N.; Florence, A. J.; Frampton, C. S. Single-crystal neutron diffraction of bio-active small molecules. *Phys. B (Amsterdam, Neth.)* **1997**, 234–236.

(70) Schantz, S.; Ljungqvist, N. Structure and dynamics in polymer blends: a ¹³C CPMAS NMR study of poly(3-octylthiophene)/poly(phenylene oxide). *Macromolecules* **1993**, *26*, 6517–6524.

(71) McBrierty, V. J.; Douglass, D. C. Recent advances in the NMR of solid polymers. *J. Polym. Sci.: Macromol. Rev.* **1981**, *16*, 295–366.

(72) Henrichs, P. M.; Tribone, J.; Massa, D. J.; Hewitt, J. M. Blend miscibility of bisphenol A polycarbonate and poly(ethylene terephthalate) as studied by solid-state high-resolution ¹³C NMR spectroscopy. *Macromolecules* **1988**, *21*, 1282–1291.

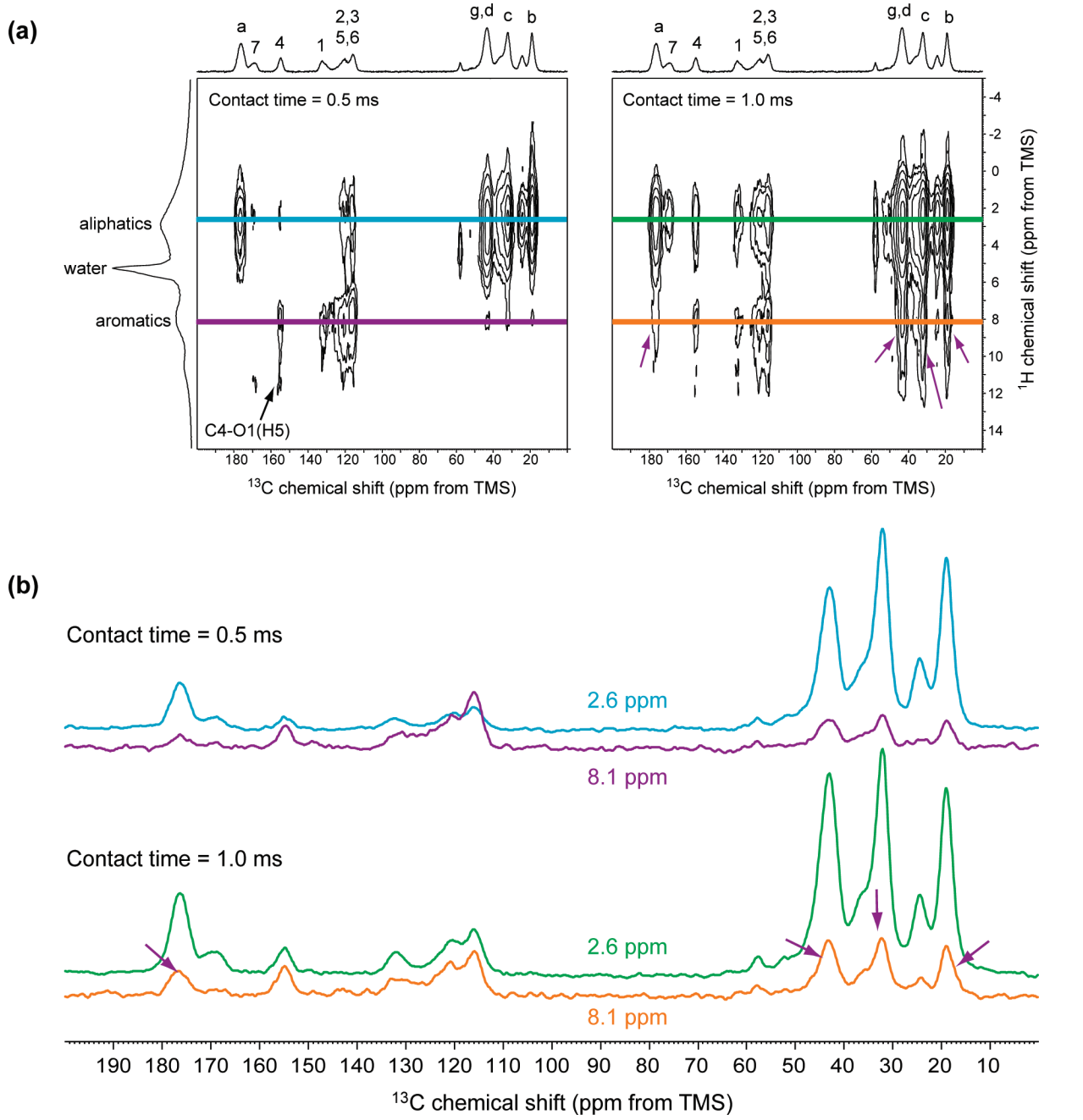

Figure 3. (a) $^{1}H-^{13}C$ CP-HETCOR spectra ($\upsilon_r = 12.5$ kHz) of amorphous dispersions of acetaminophen (**I**) in PVP (**II**), compared with the spectrum of crystalline **I** (form I). Spectra obtained with a 500 μs mixing time and a 1 ms mixing time are shown. The arrows in (a) denote a direct dipolar interaction C4−O1(H5) and spin-diffusion interactions between **I** and PVP (see text). In (b), rows extracted from the 2D spectra show the increase in intensity in the PVP signals along the rows at 8.1 ppm relative to the aliphatic signals as contact time is increased. Spectra were obtained at 9.4 T and 273 K.

lecular-level interactions that are characteristic of a glass solution. Because the correlations that are indicative of these interactions can appear as partially resolved shoulder peaks in the ^{1}H dimension, it is important to verify the result by using multiple contact times (as shown here), or using one of the two alternative approaches described below, namely, either a direct comparison with a physical mixture of amorphous drug and polymer (which is not always feasible to prepare) or a comparison of the CP-HETCOR spectrum to a LGCP-HETCOR spectrum that suppresses spin diffusion effects, as illustrated in a later section.[61]

The interaction between PVP and **I** is also detectable via ^{13}C chemical shift changes observed in the dispersion in comparison to both crystalline form I and partially amorphous **I** prepared by melt-quench in the absence of PVP (see Figure 1 and Table 1). However, the effects are subtle; only C7, C4, C1, and C8 show appreciable effects on the ^{13}C

Table 1. ^{13}C Chemical Shifts (δ) and ^{13}C-Detected ^1H T_1 Values ($\upsilon_r = 8$ kHz) of the Dispersion Containing 30% w/w Acetaminophen (**I**) in PVP Acquired at 9.4 T and 273 K[a]

assignment	δ (ppm)	$\Delta\delta_I$[b] (ppm)	$\Delta\delta_a$[c] (ppm)	T_1[d] (s)
7	169.4	−0.4	−2.0	3.74 ± 0.28
4	154.9	2.5	0.6	3.64 ± 0.13
1	132.2	−0.9	2.8	3.97 ± 0.21
3, 5	120.3			4.00 ± 0.2
2, 6	115.7	0.0	−0.1	3.35 ± 0.10
8	24.6	0.7	0.8	3.95 ± 0.17
PVP (a)	176.4			3.60 ± 0.06
PVP (g, d)	43.3			3.60 ± 0.05
PVP (f)	36.0			3.98 ± 0.19
PVP (c)	32.2			3.60 ± 0.04
PVP (b)	19.1			3.54 ± 0.05
average				
I				3.8 ± 0.3[e]
PVP				3.7 ± 0.2[e]

[a] Assignments refer to schemes **I** and **II** (PVP). [b] Change in chemical shift between crystalline form I and dispersion, $\Delta\delta_I = \delta_{dispersion} - \delta_{form\ I}$. [c] Change in chemical shift between amorphous form and dispersion, $\Delta\delta_a = \delta_{dispersion} - \delta_{amorphous}$. [d] ± estimated error from a least-squares fit to the function $y = A(1 - e^{-t/T_1})$. [e] ± standard deviation from all peaks of the solid phase.

chemical shift upon the formation of the dispersion. This illustrates a limitation of comparing spectra of amorphous material with amorphous dispersions; besides the difficulty in preparing amorphous references for some drugs, the interactions between the drug and polymer are often dominated by van der Waals forces, so that evidence of an interaction is limited to subtle changes in ^{13}C chemical shift. The $^1H-^{13}C$ CP-HETCOR experiment offers conclusive results without the need for an amorphous reference. The $^1H-^{13}C$ CP-HETCOR experiment can also provide useful structural information; in the present case, the correlations noted in Figure 3(a) suggest intermolecular interactions (most likely van der Waals forces) between aliphatic PVP and aromatic **I** positions. This agrees with atomic force microscopy studies that evaluated etching patterns of PVP−**I** dispersions and found that PVP adsorbed to the aromatic region of **I** via van der Waals forces.[73]

Evidence for molecular dissociation between PVP and **I** can be obtained from measurement of ^{13}C-detected ^1H T_1 relaxation times, as summarized in Table 1. Spin diffusion in the solid state is known to be highly efficient such that a phase pure organic material generally yields a single ^1H T_1 value at lower υ_r.[56] This is the case for **I**, which has a ^1H T_1 of >100 s, and for PVP, which has a ^1H T_1 of 0.8 s, when measured separately as pure materials. In the 30% w/w dispersion, the ^1H T_1 values measured from the ^{13}C peaks of PVP and **I** are indistinguishable, and do not show evidence of phase separation, in agreement with the $^1H-^{13}C$ CP-HETCOR results. The primary utility of the ^1H T_1 measurement is to prove phase separation by showing differences in T_1; it cannot be used to prove association definitively because of the potential occurrence of similar T_1 values for the independent materials.[40,56]

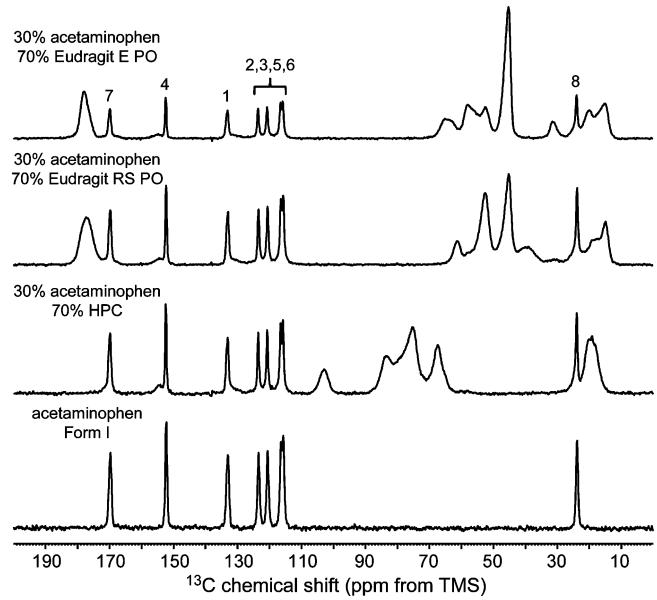

Figure 4. ^{13}C CP-TOSS spectra ($\upsilon_r = 8$ kHz) of 30% w/w dispersions of acetaminophen (**I**) in Eudragit E PO, Eudragit RS PO, and HPC, compared with the spectrum of crystalline **I** (form I). Spectra were obtained at 9.4 T and 273 K.

To illustrate the use of the ^{13}C-detected ^1H T_1 experiment in detecting phase separation, dispersions of **I** with other polymers were also prepared. In Figure 4, the ^{13}C CP-TOSS spectra of three other 30% w/w dispersions of **I** are compared with that of form I; all three dispersions show predominantly crystalline form I with small amounts of amorphous **I**. The ^{13}C-detected ^1H T_1 values for the dispersion in Eudragit RS PO (Table 2) are representative, showing two distinct species of the drug present in the dispersion; one is a crystalline phase with a narrow line width and an averaged ^1H T_1 of 2.9 ± 0.6 s, which is significantly different from the ^1H T_1 of the polymer (1.1 ± 0.2 s); the other is an amorphous phase with a broad line width and averaged ^1H T_1 of 1.2 ± 0.6 s, similar to that of the polymer. This dispersion is thus primarily a phase-separated mixture of crystalline **I** and polymer containing a small amount of a potential glass solution of **I** and Eudragit RS PO. The ^1H T_1 value of the form I in the dispersion is approximately 2 orders of magnitude lower than as-received crystalline form I, most likely because of smaller particle or domain size and enhanced form I surface area in close proximity to the polymer. The dispersions of **I** with Eudragit E PO and HPC exhibited similar ^1H T_1 behavior (not shown). In Figure 5(a), the $^1H-^{13}C$ CP-HETCOR spectrum of the dispersion of **I** and Eudragit RS PO shows the notable absence of correlations between the polymer and crystalline **I**, relative to the signals from internal spin diffusion within form I. This illustrates the results expected from a phase-separated mixture of two domains as shown by ^1H T_1 analysis. Barely detectable

(73) Wen, H.; Morris, K. R.; Park, K. Study on the interactions between polyvinylpyrrolidone (PVP) and acetaminophen crystals: Partial dissolution pattern change. *J. Pharm. Sci.* **2005**, *94*, 2166–2174.

Table 2. ^{13}C Chemical Shifts (δ) and ^{13}C-Detected ^{1}H T_1 Values for the 30% w/w Acetaminophen (**I**) Dispersion in Eudragit RS PO Acquired at 9.4 T, 273 K, and with $\upsilon_r = 8$ kHz[a]

assignment	δ (ppm)	^{1}H T_1[b] (s)
Eudragit RS PO	177.12	1.05 ± 0.02
7	169.78	3.07 ± 0.11
4 (amorphous)	155.17	0.82 ± 0.2
4	152.29	3.38 ± 0.11
1	132.98	3.35 ± 0.16
1 (amorphous)	130.44	1.63 ± 0.46
2, 3, 5, 6	123.37	3.25 ± 0.09
2, 3, 5, 6	120.56	3.09 ± 0.1
2, 3, 5, 6	116.38	3.06 ± 0.14
2, 3, 5, 6	115.66	2.96 ± 0.11
Eudragit RS PO	61.27	1.12 ± 0.05
Eudragit RS PO	52.65	1.07 ± 0.01
Eudragit RS PO	45.36	1.07 ± 0.02
Eudragit RS PO	39.04	1.07 ± 0.05
Eudragit RS PO	31.38	1.59 ± 0.58
8	23.82	2.59 ± 0.11
Eudragit RS PO	19.86	1.04 ± 0.05
Eudragit RS PO	17.6	1.13 ± 0.08
average		
I, crystalline		2.9 ± 0.6[c]
I, amorphous		1.2 ± 0.6[c]
Eudragit RS PO		1.1 ± 0.2[c]

[a] Assignments refer to scheme **I**. [b] ± estimated error from a least-squares fit to the function $y = A(1 - e^{-t/T_1})$. [c] ± standard deviation from all peaks of the solid phase.

signals in the extracted rows at $F_1 = 5.0$ ppm in Figure 5(b) align with the minor amorphous phase and not the crystalline peaks, but are too weak to definitively confirm that the minor phase is a glass solution of **I** and Eudragit RS PO.

Indomethacin−PVP Dispersions. Indomethacin was chosen to be representative of a more typical small molecule drug with greater structural complexity than **I**.[23,25,74] A recent SSNMR analysis of indomethacin-PVP 1:4 w/w solid dispersions made use of ^{13}C-detected ^{1}H $T_{1\rho}$ measurements to assess molecular mobility, as these values are sensitive to slower motions of amorphous materials,[75] but did not include a temperature study to address thermal effects on relaxation times.[76] The structure and SCXRD numbering scheme of indomethacin are shown in **III**, with the numbering scheme taken from the crystal structure of the γ-polymorph (CSD refcode INDMET03).[77]

A ^{13}C CP-TOSS spectrum of the input γ-polymorph, with its phase identity confirmed by PXRD (see Supporting Information), is shown in Figure 6. Peak assignments are based on previous work, a dipolar dephasing experiment, and ^{1}H−^{13}C CP-HETCOR data (see Supporting Information).[32,78,79] Figure 6 also shows the ^{13}C spectrum of a 30% w/w dispersion of **III** in PVP prepared using fast evaporation

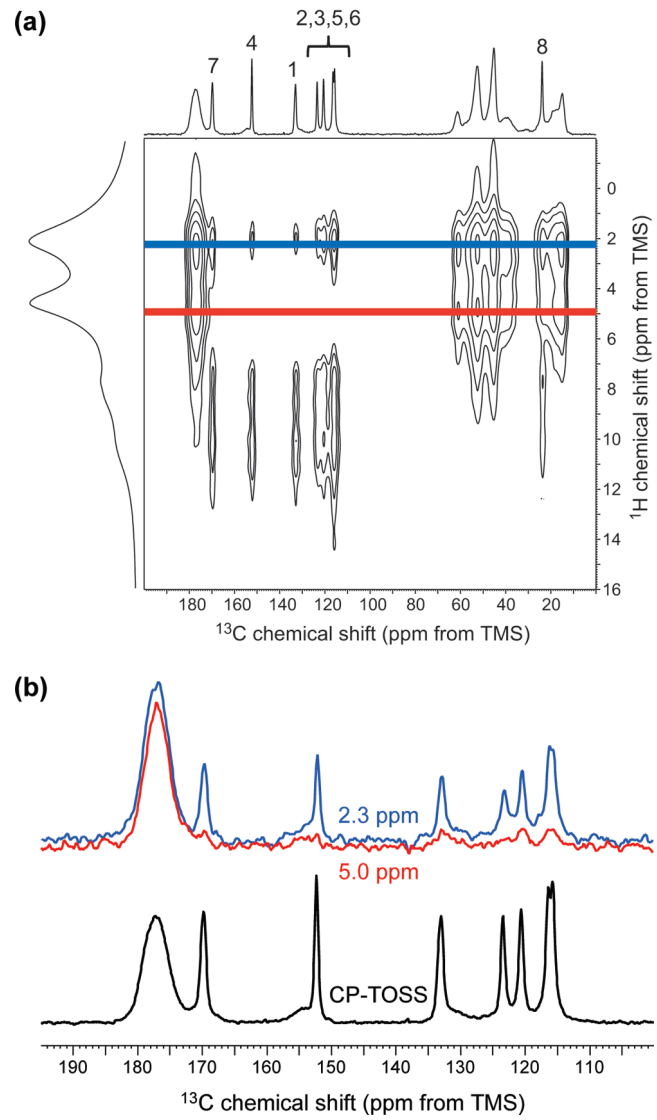

Figure 5. (a) ^{1}H−^{13}C CP-HETCOR spectrum ($\upsilon_r = 12.5$ kHz) of the dispersion of acetaminophen (**I**) in Eudragit RS PO polymer, obtained using a 2 ms contact time. This dispersion contains phase-separated domains of form I (see text and Table 2). The ^{1}H MAS spectrum ($\upsilon_r = 35$ kHz) and ^{13}C CP-TOSS spectrum ($\upsilon_r = 8$ kHz) are shown as the F_1 and F_2 projections, respectively. (b) Extractions of rows from the spectrum in (a) (each a sum of 10 rows), showing the lack of spectral intensity for crystalline **I** in the $F_1 = 5$ ppm region (red spectrum) consistent with separated domains; only weak signals are observed that are consistent with the low-level amorphous phase seen in the ^{13}C spectrum. Internal spin diffusion within **I** can be seen at $F_1 = 2.3$ ppm (blue spectrum), and the ^{13}C CP-TOSS spectrum is shown for comparison. Spectra were obtained at 9.4 T and 273 K.

(74) Yoshioka, M.; Hancock, B. C.; Zografi, G. Inhibition of indomethacin crystallization in poly(vinylpyrrolidone) coprecipitates. *J. Pharm. Sci.* **1995**, *84*, 983–986.
(75) Guilbaud, J. B.; Cummings, L.; Khimyak, Y. Encapsulation of indomethacin in PVP: solid-state NMR studies. *Macromol. Symp.* **2007**, *251*, 41–46.
(76) Levitt, M. H. *Spin dynamics: Basics of nuclear magnetic resonance*; John Wiley & Sons: Chichester, 2001; pp 513–538.

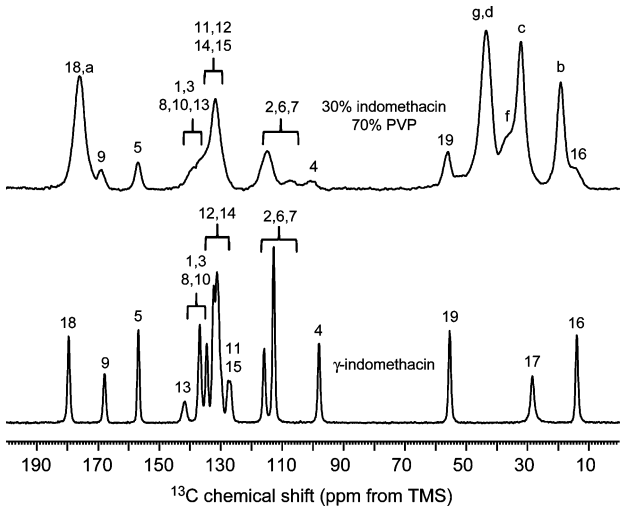

Figure 6. ^{13}C CP-TOSS spectrum (υ_r = 8 kHz) of a 30% w/w amorphous dispersion of indomethacin (**III**) in PVP compared with the spectrum of crystalline γ-indomethacin. Peak assignments refer to schemes **II** (PVP) and **III**. The peak associated with C13 in the γ-form is the high-frequency component of the chlorinated carbon, split by residual dipolar−quadrupolar interactions (see text and ref 79). Spectra were obtained at 9.4 T and 273 K.

III

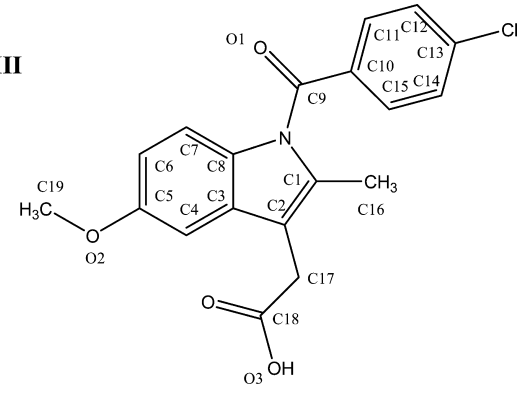

from dichloromethane. This dispersion has previously been shown to be a glass solution by both DSC and PDF-PXRD analysis.[23,25,74] As in the PVP dispersion of **I**, the ^{13}C spectrum offers evidence that the drug is amorphous through the broad signals observed in the spectrum. As with **I**, ^{13}C resonances of **III** in the dispersion are shifted relative to the crystalline form (Table 3). These changes in chemical shifts highlight the different environment for **III** in the dispersion relative to the γ-polymorph. The resonances of PVP do not change significantly (Table 3), which is expected given the molar ratio of 10 monomer units of PVP to 1.3 molecules of **III**. The association of **III** with PVP in a glass solution can again be shown via spin diffusion effects in ^{1}H−^{13}C CP-HETCOR spectra, as depicted in Figure 7(a). As PVP contains no aromatic protons, the correlations from the aliphatic carbons of PVP to the protons with aromatic chemical shifts, highlighted on the spectrum, unambiguously confirms molecular contact between the two components of the dispersion. Comparison of data acquired with short (500 μs) and long (2 ms) contact times in Figure 7(a) shows the increase in correlations from spin diffusion (denoted by arrows). Unlike the case with **I**, it was possible to prepare a stable 30% w/w physical mixture of amorphous **III** and PVP and further confirm that the key ^{1}H−^{13}C CP-HETCOR correlations between **III** and PVP arise from spin diffusion. The results are shown in Figure 7(b); direct comparison of the 2 ms contact time spectra for the physical mixture and the dispersion clearly shows that the correlations marked with arrows are not present in the physical mixture, as expected. The unambiguous results of the ^{1}H−^{13}C CP-HETCOR experiments contrast with the subtle changes in the ^{13}C CP-TOSS spectra between the dispersion and physical mixture (see Supporting Information) and highlight the utility of this method of demonstrating glass solution formation. Finally, ^{13}C-detected ^{1}H T_1 values measured for **III** and PVP are reported in Table 3, and yielded 5.9 ± 0.3 s and 6.0 ± 0.2 s for the drug and polymer, respectively. These values agree within the range of experimental error, and show no evidence of phase separation between the drug and PVP.

In previous work, vibrational spectroscopy was used to show that the 30% w/w dispersion of **III** in PVP does not

Table 3. ^{13}C Chemical Shifts (δ) and ^{13}C-Detected ^{1}H T_1 Values for the Dispersion Containing 30% w/w Indomethacin (**III**) in PVP Obtained at 9.4 T, 273 K, and with υ_r = 8 kHz[a]

assignment	δ (ppm)	$\Delta\delta^b$ (ppm)	^{1}H $T_1{}^c$ (s)
18	176.1	−3.5	
9	169.3	1.4	
5	157.0	0.1	
aromatic	138.3		6.2 ± 0.5
aromatic	131.8		5.9 ± 0.2
2, 7, 6	115.1	−1.0, 2.2	5.9 ± 0.3
7, 6, 4	107.1	−5.8, 9.1	
4	100.5	2.4	
19	56.4	0.9	5.6 ± 0.5
16	14.1	0.2	
PVP (a)	176.1	−0.5	5.9 ± 0.1
PVP (g, d)	43.8	0.1	6.0 ± 0.1
PVP (f)	36.9	0.0	6.4 ± 0.4
PVP (c)	32.2	0.0	6.0 ± 0.1
PVP (b)	19.1	0.0	5.9 ± 0.1
average			
III			5.9 ± 0.3[d]
PVP			6.0 ± 0.2[d]

[a] Assignments refer to schemes **III** and **II** (PVP). [b] Pure-phase to dispersion change in chemical shift, $\Delta\delta = \delta_{dispersion} - \delta_{pure\text{-}phase}$. [c] ± estimated error from a least-squares fit to the function $y = A(1 - e^{-t/T_1})$. [d] ± standard deviation from all peaks of t he solid phase.

(77) Cox, P. J.; Manson, P. L. γ-Indomethacin at 120 K. *Acta Crystallogr.* **2003**, *E59*, o986−o988.

(78) Masuda, K.; Tabata, S.; Kono, H.; Sakata, Y.; Hayase, T.; Yonemochi, E.; Terada, K. Solid-state ^{13}C NMR study of indomethacin polymorphism. *Int. J. Pharm.* **2006**, *318*, 146–153.

(79) Apperley, D. C.; Forster, A. H.; Fournier, R.; Harris, R. K.; Hodgkinson, P.; Lancaster, R. W.; Rades, T. Characterisation of indomethacin and nifedipine using variable-temperature solid-state NMR. *Magn. Reson. Chem.* **2005**, *43*, 881–892.

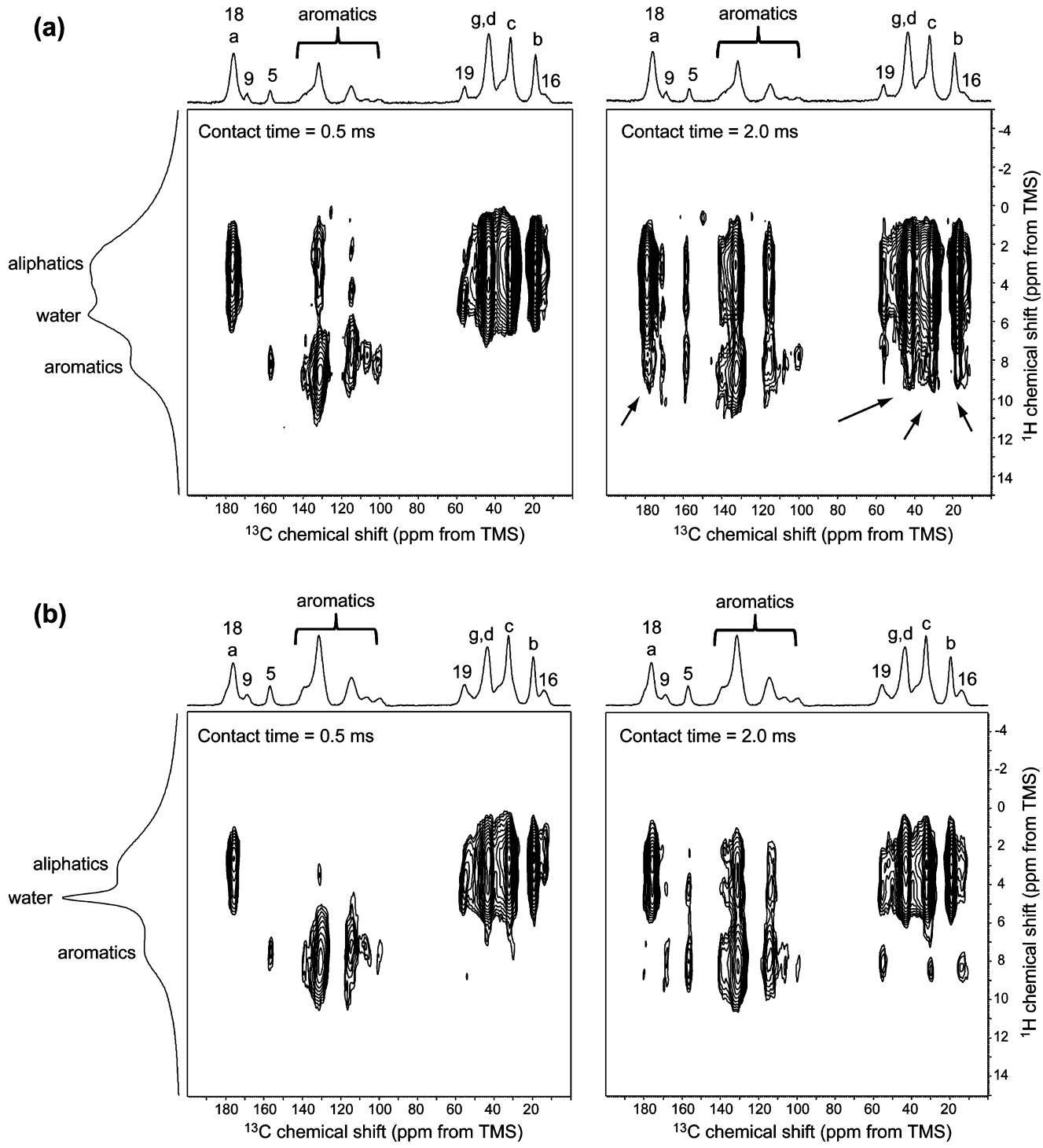

Figure 7. (a) $^{1}H-^{13}C$ CP-HETCOR spectra (υ_r = 12.5 kHz) of a 30% w/w dispersion of indomethacin (**III**) in PVP obtained with 500 μs and 2 ms contact times. The arrows denote spin-diffusion interactions between **III** and PVP (see text). In (b), $^{1}H-^{13}C$ CP-HETCOR spectra obtained under identical conditions are shown for a 30% w/w physical mixture of amorphous **III** in PVP, showing the lack of spin diffusion correlations between **III** and PVP. 2D contours are drawn starting just above the noise floor with extra levels used to capture small correlations. The ^{1}H MAS spectra (υ_r = 35 kHz) and ^{13}C CP-TOSS spectra (υ_r = 8 kHz) are shown as the F_1 and F_2 projections, respectively. Spectra were obtained at 9.4 T and 273 K.

maintain the dimeric hydrogen bonding motif involving the carboxylic acid group, as seen for example in the crystal structure of the γ-polymorph.[25,77] However, this approach requires that the absence of hydrogen bonding be inferred by comparison of the spectral properties of the dispersion and the known crystalline forms.[25] It also involved the use of acetic acid and methylpyrrolidone as models for **III** and PVP, respectively, to aid in the interpretation of the Raman

and IR spectra of **III**−PVP dispersions.[25] ^{1}H SSNMR offers a more direct approach to disproving a dimeric interaction. The ^{1}H MAS spectrum of the 30% w/w dispersion of **III**, shown plotted along the F_1 dimension in Figure 7(a), shows a small amount of spectral intensity in the hydrogen-bonding region (between 10 and 13 ppm) that could be a hydrogen-bonding position. By using a ^{1}H DQ-BABA experiment, which highlights dimeric carboxylate interactions through the close spatial proximity (typically 2.5 Å) of protons engaged in the interaction,[59,80] evidence for the absence of dimeric interactions in the dispersion can be readily obtained without recourse to reference samples or model spectra. In Figure 8(a), the DQ-BABA spectrum of the 30% w/w dispersion of **III** in PVP is shown. The absence of an autocorrelation peak at a DQ frequency in the range of 20−30 ppm indicates the lack of dimeric carboxylate hydrogen bonding. In contrast, an autocorrelation peak indicative of a dimeric carboxylate interaction is clearly seen in the DQ-BABA spectrum of the γ-polymorph of **III** in Figure 8(b). The amorphous forms of **III** are also known to exhibit the dimeric carboxylate interaction in some cases, depending on the manner in which they are prepared.[81] The DQ-BABA experiment can detect these interactions, if present, in amorphous materials, and should be highly useful for studies of dispersions wherein the drug is known to favor such interactions in crystalline phases. A correlation between aromatic and aliphatic positions is also observed in the DQ-BABA spectrum in Figure 8(a), which could be intramolecular interactions within **III** or intermolecular interactions between **III** and PVP; poor resolution limits any additional interpretation, showing the need for complementary ^{13}C-based experiments (e.g., ^{1}H−^{13}C CP-HETCOR) to prove molecular association.

The crystalline γ-polymorph of **III** shows a hydrogen-bonding resonance at 13.8 ppm in its ^{1}H spectrum, assigned to H1(O3) via a ^{1}H−^{13}C CP-HETCOR experiment (see Supporting Information). A deshielded resonance in the ^{1}H DP-MAS spectrum of the 30% w/w dispersion of **III** in PVP is observed as a poorly resolved shoulder in Figures 7 and 8. In order to more clearly determine the chemical shift of this proton, the dispersion was exchanged in a 75% RH D_2O environment to cause exchange at the carboxylic acid, and then quickly vacuum-dried and analyzed by a ^{2}H DP-MAS experiment (see Supporting Information). The carboxylic acid deuteron resonated at a chemical shift of 13.0 ppm, yielding the shift of H1(O3) in the solid dispersion and indicating that this group is likely engaged in a hydrogen bond to PVP,

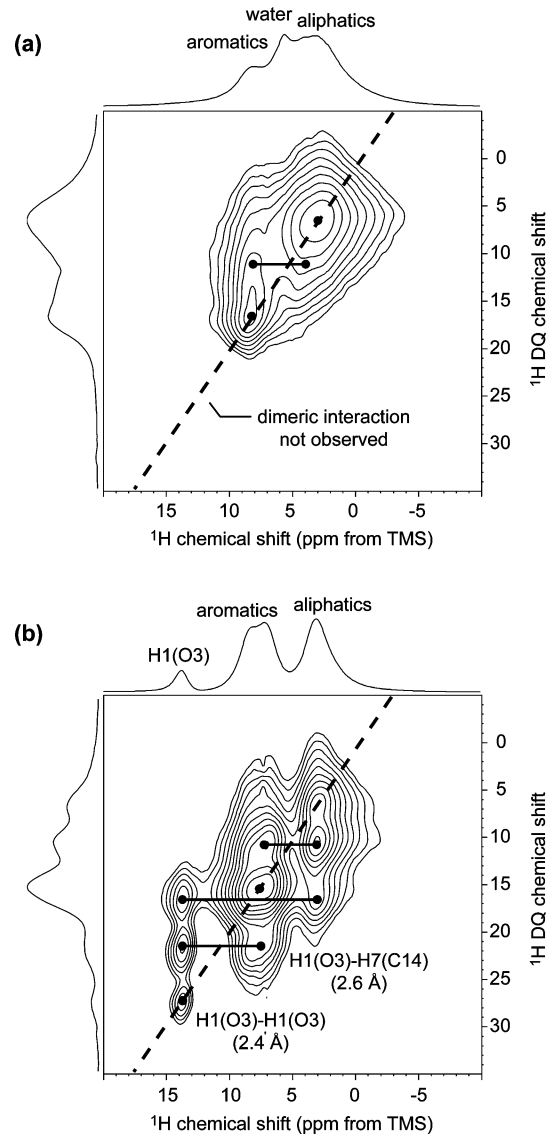

Figure 8. ^{1}H DQ-BABA spectra (υ_r = 35 kHz) of (a) the 30% w/w amorphous dispersion of indomethacin (**III**) in PVP and (b) the crystalline γ-form. The horizontal bars denote DQ correlations of interest (see text). The distances shown in (b) are taken from the crystal structure (ref 77). The ^{1}H MAS spectra (υ_r = 35 kHz) are plotted along the F_2 axes and double-quantum skyline projections are shown along the F_1 axes. Spectra were obtained at 9.4 T and 273 K.

with a predicted length of 1.64 ± 0.04 Å from eq 1. However, direct evidence for a hydrogen bonding interaction between **III** and PVP, namely, Ca═O···H1(O3), could not be clearly detected in the ^{1}H−^{13}C CP-HETCOR spectra in Figure 7(a).

Trehalose−Dextran Dispersions. Dispersions of trehalose and dextran have been shown by PDF-PXRD and DSC to be solid nanosuspensions, containing domains of nanometer size of one component within the other.[23] The numbered structures of trehalose and dextran are presented in schemes **IV** and **V**, respectively. Solid nanosuspensions of crystalline or amorphous drug represent an extreme case of materials

(80) Vogt, F. G.; Katrincic, L. M.; Long, S. T.; Mueller, R. L.; Carlton, R. A.; Sun, Y. T.; Johnson, M. N.; Copley, R. C. B.; Light, M. E. Enantiotropically-related polymorphs of {4-(4-chloro-3-fluorophenyl)-2-[4-(methyloxy)phenyl]-1,3-thiazol-5-yl} acetic acid. Crystal structures and multinuclear solid-state NMR. *J. Pharm. Sci.* **2008**, *97*, 4756–4782.

(81) Savolainen, M.; Heinz, A.; Strachan, C.; Gordon, K. C.; Yliruusi, J.; Rades, T.; Sandler, N. Screening for differences in the amorphous state of indomethacin using multivariate visualization. *Eur. J. Pharm. Sci.* **2007**, *30*, 113–123.

often referred to as "eutectic mixtures".[5,13] For each of the dispersions a single increasing value of T_g was observed with decreasing **IV** content, while PDF-PXRD measurements suggested contributions from two separated domains of **IV** and **V**.[23] Since a single value of T_g indicates domain sizes of 30 nm or less, it was concluded that the **IV** and **V** dispersions were nanosuspensions containing domains with sizes estimated to be on the order of nanometers.[23] Domain sizes of heterogeneous systems such as polymer blends can be measured by using spin diffusion experiments, which have been described in detail previously.[27,37,82,83] The basic spin diffusion experiment involves a selective excitation of one phase of the heterogeneous system followed by a variable mixing delay to allow spin diffusion to transfer to other phases. The selective excitation step can be adapted for the application using a double-quantum filter to select a rigid phase,[84] a dipolar filter to select a mobile phase,[85] or a filter to select a particular chemical shift range.[27,86] Though the spin diffusion experiment can provide an accurate measurement of domain size, it is a relatively elaborate analysis, involving acquisition of multiple 1D or 2D spectra and fitting them to an analytical function or an initial buildup rate.[27] A simpler alternative is to estimate the upper limit of the domain size by using the diffusion-averaged relaxation time of ^{1}H T_1 or ^{1}H $T_{1\rho}$. This can be achieved by use of eq 2, where L is related to D and t (in this case ^{1}H T_1 or ^{1}H $T_{1\rho}$).[70−72] If the domain size is small compared to L, spin diffusion will average the relaxation times of all protons from different domains to a single value.[56,72] If instead the domain size is large compared to L, the components retain their distinctive relaxation times.[56,70,72]

Figure 9 shows ^{13}C CP-TOSS spectra of 30 and 50% w/w dispersions of **IV** in **V**, with characteristic peaks noted for carbons 1, 1′, a, and a′. For systems not exhibiting molecular dynamics, D can be increased by reducing υ_r and varied to help estimate domain size.[87] The ^{1}H T_1 relaxation times were measured with υ_r set to 5 and 14 kHz and are summarized in Table 4. For the 50% w/w dispersion, the ^{1}H T_1 values measured with $\upsilon_r = 14$ kHz are clearly different for **IV** and **V**, indicating that L is small compared to domain size. By

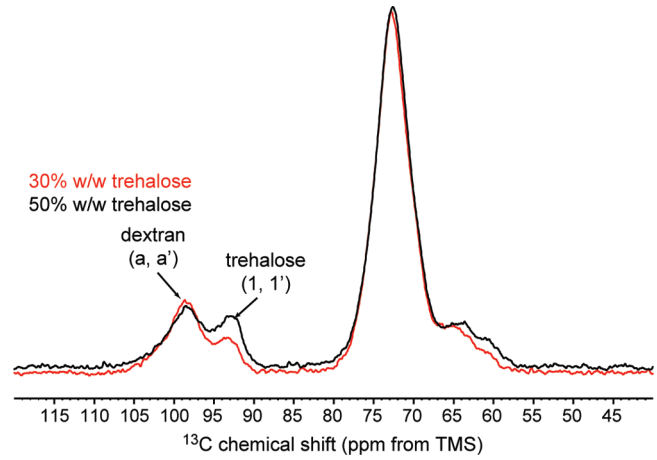

Figure 9. ^{13}C CP-TOSS spectra (υ_r = 8 kHz) of two dispersions of trehalose (**IV**) and dextran (**V**). The spectrum of the sample containing 50% w/w **IV** is shown in black, while the spectrum of the 30% w/w **IV** sample is shown in red. Characteristic peaks for dextran and trehalose are marked with arrows. Spectra were obtained at 8.5 T and 273 K.

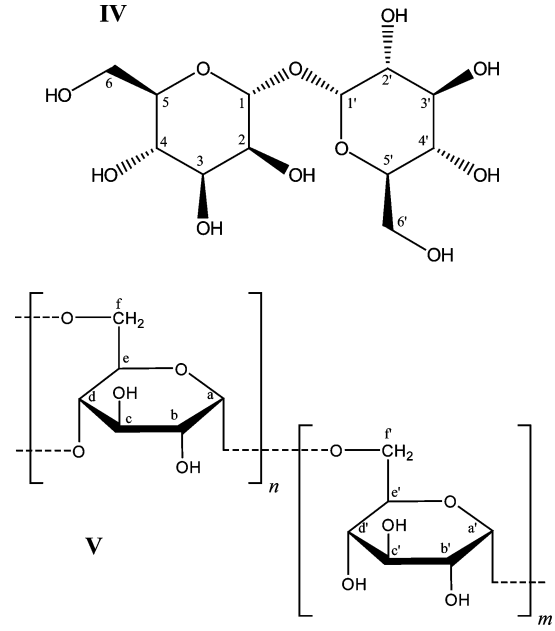

reducing υ_r to 5 kHz for the 50% w/w dispersion, the ^{1}H T_1 of **IV** and **V** averaged to a single value of about 9 s. With $T_2 = 80$ μs measured from the ^{1}H line width, eq 2 yields an L of 82 nm. Therefore, the averaged ^{1}H T_1 at 5 kHz MAS rate indicates a domain size for **IV** of less than 82 nm, consistent with previous reports.[23] For the 30% w/w dispersion, υ_r had a lesser effect on the spin diffusion coefficient as ^{1}H T_1 averaged to approximately 4 s with υ_r set to both 5 and 14 kHz, thus indicating a **IV** domain size of less than 55 nm. It should be emphasized that these upper limits for

(82) Vanderhart, D. L.; McFadden, G. B. Some perspectives on the interpretation of proton NMR spin diffusion data in terms of polymer morphologies. *Solid State Nucl. Magn. Reson.* **1996**, *7*, 45–66.
(83) Demco, D. E.; Johansson, A.; Tegenfeldt, J. Proton spin diffusion for spatial heterogeneity and morphology investigations of polymers. *Solid State Nucl. Magn. Reson.* **1995**, *4*, 13–38.
(84) Cherry, B. R.; Fujimoto, C. H.; Cornelius, C. J.; Alam, T. M. Investigation of domain size in polymer membranes using double-quantum-filtered spin diffusion magic angle spinning NMR. *Macromolecules* **2005**, *38*, 1201–1206.
(85) Marjanski, M.; Srinivasarao, M.; Mirau, P. A. Solid-state multiple proton nuclear magnetic resonance (NMR) characterization of self-assembling polymer films. *Solid State Nucl. Magn. Reson.* **1998**, *12*, 113–118.
(86) Schmidt-Rohr, K.; Clauss, J.; Blümich, B.; Spiess, H. W. Miscibility of polymer blends investigated by ^{1}H spin diffusion and ^{13}C NMR detection. *Magn. Reson. Chem.* **1990**, *28*, 3–9.
(87) Krushelnitsky, A.; Brauniger, T.; Reichert, D. ^{15}N spin diffusion rate in solid-state NMR of totally enriched proteins: The magic angle spinning frequency effect. *J. Magn. Reson.* **2006**, *182*, 339–342.

Table 4. ^{13}C Chemical Shifts (δ) and ^{13}C-Detected ^{1}H T_1 Values for Trehalose (**IV**) and Dextran (**V**) Dispersions Acquired at 8.4 T, 273 K, and Two Spinning Rates (υ_r = 14 and 5 kHz)

assignment	δ (ppm)	^{1}H T_1[a] (s)	$\Delta(^1\text{H } T_1)$[b,c] (s)
50% w/w Trehalose Dispersion			
		υ_r = 14 kHz	
dextran	98.1	6.29 ± 0.23	
trehalose	92.6	5.42 ± 0.27	0.87 ± 0.35
		υ_r = 5 kHz	
dextran	98.1	8.98 ± 0.18	
trehalose	92.6	8.61 ± 0.29	0.37 ± 0.34
30% w/w Trehalose Dispersion			
		υ_r = 14 kHz	
dextran	98.5	3.53 ± 0.09	
trehalose	92.8	4.14 ± 0.44	0.61 ± 0.45
		υ_r = 5 kHz	
dextran	98.5	4.36 ± 0.18	
trehalose	92.8	4.15 ± 0.46	0.21 ± 0.49

[a] ± estimated error from least-squares fit to the function $y = A(1 - e^{-t/T_1})$. [b] $\Delta(^1\text{H } T_1) = |^1\text{H } T_{1\text{trehalose}} - ^1\text{H } T_{1\text{dextran}}|$. [c] $\pm\Delta(^1\text{H } T_1)$ calculated as propagation of the two estimated errors; see ref 58.

domain sizes may be overestimated because of overlapped ^{1}H signals between **IV** and **V** affecting the measured ^{1}H line width, and that the domains may actually be closer to the 30 nm range estimated previously.[23] However, the SSNMR approach provides a useful upper limit to domain size for nanosuspension systems, and can be applied to complex systems containing multiple polymers.

Diflunisal Dispersions. Fluorinated drug molecules are common in modern drug development, with many experimental molecules in the clinic and a large number of marketed examples.[88] When fluorine is present, the sensitivity of ^{19}F SSNMR makes it a preferred mode of analysis for amorphous dispersions.[45] To illustrate the use of 2D SSNMR techniques in the characterization of amorphous dispersions of fluorinated APIs, a model system containing diflunisal and PVP is utilized. Diflunisal (**VI**) is a marketed prostaglandin-inhibiting nonsteroidal anti-inflammatory drug.[89] The numbering scheme of **VI** is taken from the crystal structure (CSD refcode FAFWIS01).[90]

VI

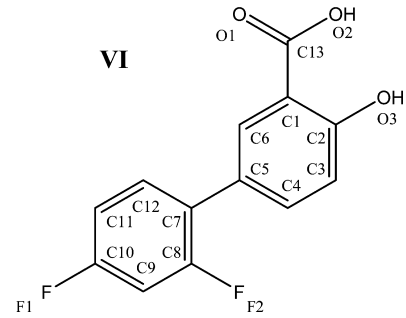

Crystalline **VI** is known to exist in multiple polymorphic forms which are sparingly soluble in water.[90−93] The most thermodynamically stable of the known forms[92] corresponds to CSD refcode FAFWIS01, and is referred to as form I by some authors[90,91] and form A by others.[92] Previous studies of **VI** in amorphous dispersions have included an amorphous, salt-like coprecipitate with cimetidine[94] and a study of dispersions of **IV** with Eudragit RS and RL polymers.[12] The latter study includes ^{13}C SSNMR analysis of dispersions, which were primarily crystalline input material, as well as ^{1}H T_1 analysis to demonstrate a large difference in domain size between the dispersed drug and the crystalline input material.[12] To our knowledge, no ^{19}F SSNMR studies of **VI**-containing systems have been reported. In the present work, dispersions of **VI** in PVP were prepared by rapid solvent evaporation from ethanol.[46] This dispersion has been previously reported to be a glass solution at lower drug concentrations from the results of DSC studies.[46] The input form used to prepare this dispersion was confirmed to be form I (form A) by PXRD analysis, and matched the pattern predicted from the FAFWIS01 crystal structure (see Supporting Information).[90−92] Both 30% and 80% w/w dispersions were prepared, the latter to intentionally overload the polymer and create domains of crystalline material for comparison.[46]

The ^{13}C CP-TOSS spectrum of form I of **VI** is compared to the spectra of the 30% and 80% w/w amorphous dispersions in Figure 10(a). The ^{13}C spectrum of crystalline form I matches that previously reported.[12] The spectra shown were obtained with only ^{1}H decoupling; the use of dual ^{1}H/^{19}F decoupling did not improve the results for the amorphous dispersion because of the broad carbon linewidths. Dual ^{1}H/^{19}F decoupling also did not significantly improve the spectrum of crystalline form 1. This is likely the result of dynamic broadening effects; preliminary variable temperature studies of form I using both ^{13}C and ^{19}F SSNMR showed a

(88) Böhm, H.-J.; Banner, D.; Bendels, S.; Kansy, M.; Kuhn, B.; Müller, K.; Obst-Sander, U.; Stahl, M. Fluorine in medicinal chemistry. *ChemBioChem* **2004**, *5*, 637–643.

(89) Steelman, S. L.; Cirillo, V. J.; Tempero, K. F. The chemistry, pharmacology and clinical pharmacology of diflunisal. *Curr. Med. Res. Opin.* **1978**, *5*, 506–514.

(90) Cross, W. I.; Blagden, N.; Davey, R. J.; Pritchard, R. G.; Neumann, M. A.; Roberts, R. J.; Rowe, R. C. A whole output strategy for polymorph screening: Combining crystal structure prediction, graph set analysis, and targeted crystallization experiments in the case of diflunisal. *Cryst. Growth Des.* **2003**, *3*, 151–158.

(91) Martínez-Ohárriz, C.; Martín, C.; Goñi, M. M.; Rodríguez-Espinosa, C.; Tros De Ilarduya-Apaolaza, M. C.; Sánchez, M. Polymorphism of diflunisal: Isolation and solid-state characteristics of a new crystal form. *J. Pharm. Sci.* **1994**, *83*, 174–177.

(92) Perlovich, G. L.; Hansen, L. K.; Bauer-Brandl, A. Interrelation between thermochemical and structural data of polymorphs exemplified by diflunisal. *J. Pharm. Sci.* **2002**, *91*, 1036–45.

(93) Cotton, M. L.; Hux, R. A. Diflunisal. *Anal. Profiles Drug Subst.* **1985**, *14*, 491–526.

(94) Yamamura, S.; Gotoh, H.; Sakamoto, Y.; Momose, Y. Physicochemical properties of amorphous salt of cimetidine and diflunisal system. *Int. J. Pharm.* **2002**, *241*, 213–221.

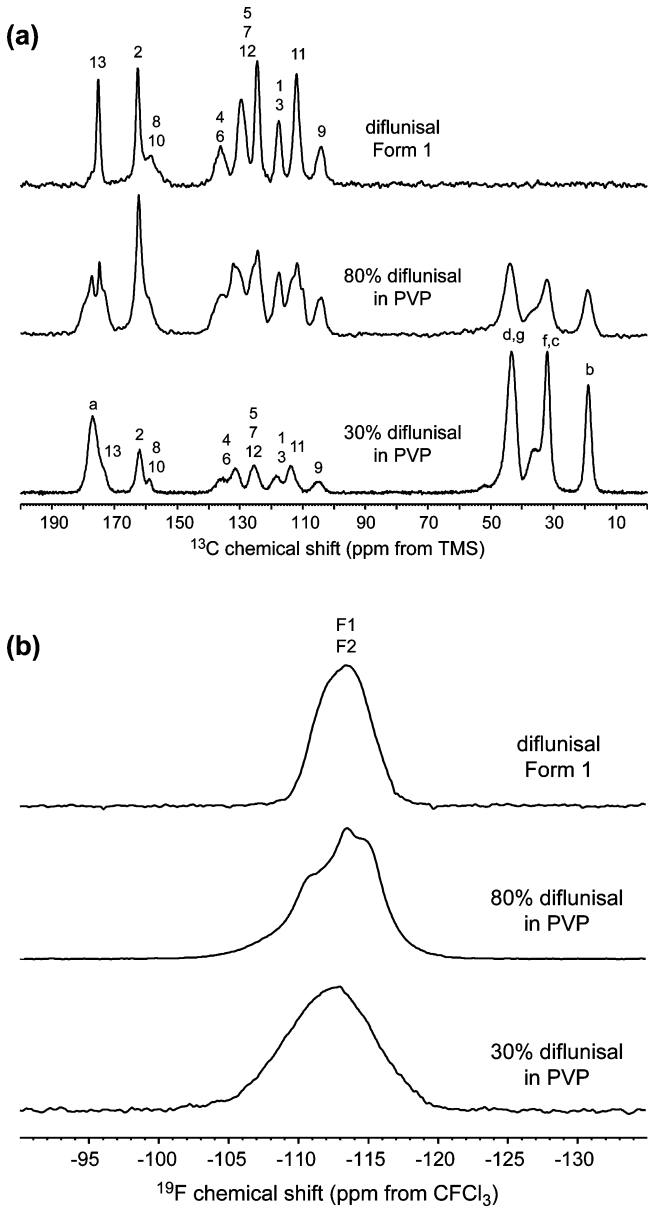

Figure 10. (a) ^{13}C CP-TOSS spectra ($\upsilon_r = 8$ kHz) of 30% and 80% w/w dispersions of diflunisal (**VI**) in PVP compared with crystalline form 1 of **VI**. (b) ^{19}F CP-MAS spectra ($\upsilon_r = 12.5$ kHz) of the same dispersions and form 1. Spectra were obtained at 9.4 T and 273 K.

temperature dependent line shape indicative of motion involving the fluorinated ring, consistent with the disorder observed for the F2 position in the crystal structure.[90] The ^{13}C spectrum of the 30% w/w dispersion is indicative of amorphous material, in agreement with previous PXRD studies, while the spectrum of the 80% w/w dispersion shows a mixture of crystalline and amorphous drug. The crystalline component of the PXRD pattern of the 80% w/w dispersion did not match with the reported patterns, but did resemble the pattern predicted for form III via the FAFWIS02 structure (see Supporting Information).[90]

The expanded centerband regions of the ^{19}F spectrum of form 1 of **VI** and the 30% and 80% w/w amorphous dispersions are shown in Figure 10(b). The form 1 spectrum is broadened by the aforementioned disorder in the crystal structure involving F_2, and spectral overlap between F_1 and F_2. Thus, the ^{19}F spectrum of the amorphous dispersion is only slightly broader than that of form 1. The 80% w/w sample thus illustrates the lack of resolution that may occasionally limit ^{19}F SSNMR analysis. If a spectrum of only the amorphous component is desired, this can be overcome using spectral editing approaches that rely on T_1, $T_{1\rho}$, or T_2 for either ^{1}H or ^{19}F nuclei, as discussed further below. Fortunately, cases of such severe overlap are not often observed; another fluorinated drug molecule discussed below, for example, shows more typical partially resolved spectra.

The ^{1}H MAS and DQ-BABA spectra of the 30% w/w amorphous dispersion of **VI** are compared to those of crystalline form 1 in Figure 11. As in the case of the PVP dispersion of **III**, the DQ-BABA spectrum in Figure 11(a) immediately shows that intermolecular dimeric interactions between the carboxylate groups and also between the hydroxyl groups in the FAFWIS01 structure are lost (Figure 11(b)). The lack of aliphatic protons in **VI** allows for observation of close-contact (~3 Å) intermolecular dipolar interactions in Figure 11(a) between aliphatic PVP protons and the deshielded H2(O2), H1(O3), and aromatic protons in **VI**. The DQ-BABA experiment also observes several intramolecular interactions in the dispersion between the H2(O2) and H1(O3) positions and aromatic groups. This is an interesting but atypical case; as previously noted, the short range and limited resolution of the ^{1}H DQ-BABA experiment, which does not allow for spin diffusion, generally precludes the detection of drug−polymer interactions and limits its use to intramolecular effects.

Although the ^{19}F spectra of **VI** and its dispersions lack the high resolution often seen in ^{19}F spectra of crystalline compounds, ^{1}H−^{19}F CP-HETCOR experiments can be readily used to confirm the formation of an amorphous glass solution. The spectra of the 30% w/w dispersion shown in Figure 12(a) illustrate the approach. Using a short 100 μs mixing time, correlations are observed between the fluorine signal and both aromatic and aliphatic protons; the latter can only be associated with PVP, confirming the interactions seen in the ^{1}H DQ-BABA spectrum. The correlation to aromatic protons increases markedly with a 2 ms contact time as expected from spin diffusion. As noted previously, CP-HETCOR data from a dispersion and a physical mixture can be compared to confirm spin diffusion, or in the more typical case where an amorphous physical mixture cannot be prepared, CP-HETCOR data at different mixing times can be compared to identify spin diffusion correlations. Another approach to confirming spin diffusion effects is possible using the LGCP method, which greatly reduces spin diffusion during the ^{1}H spin lock period. This approach is demonstrated for the 30% w/w dispersion of **VI** in PVP in Figure 12(b). As shown by the relative intensity of the correlations, the buildup of spin diffusion is eliminated; the remaining correlation between the fluorine signals and aliphatic protons

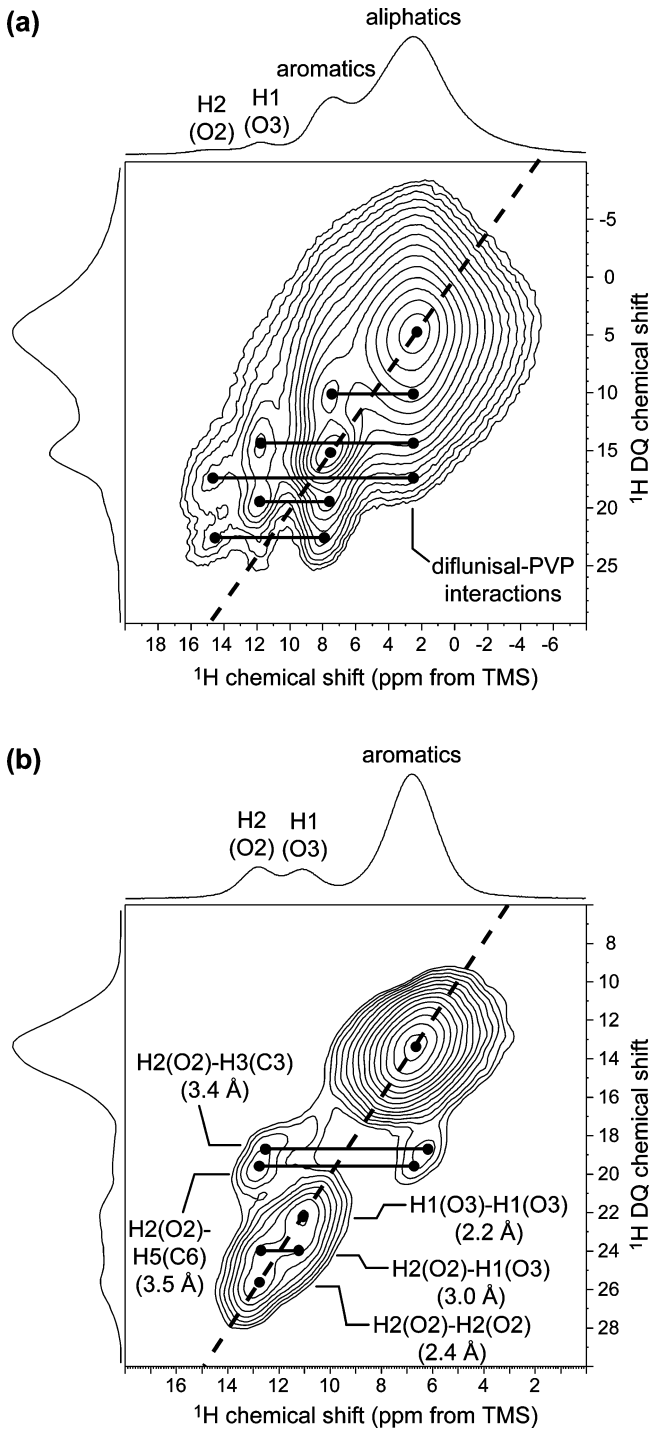

Figure 11. ^{1}H DQ-BABA spectra (υ_r = 35 kHz) of (a) the 30% w/w amorphous dispersion of diflunisal (**VI**) in PVP and (b) crystalline form 1 of **VI**. The spectrum in (a) shows interactions between H1, H2, and aromatic signals and the aliphatic PVP signals. The ^{1}H MAS spectra (υ_r = 35 kHz) are plotted along the F_2 axes and double-quantum skyline projections are shown along the F_1 axes. The distances shown in (b) are taken from the crystal structure (ref 90). Spectra were obtained at 11.7 T and 273 K.

can then be assigned to a direct through-space dipolar interaction. The ^{1}H−^{19}F CP-HETCOR and LGCP-HETCOR spectra each required about four hours of acquisition time to obtain, and alone are sufficient to show the formation of a glass solution in this case. As a result, there is no need to utilize the less sensitive ^{1}H−^{13}C CP-HETCOR experiment.

The partially crystalline nature of the 80% w/w dispersion of **VI** provides an opportunity to demonstrate another useful SSNMR approach for determining whether the crystalline component is a single phase, beyond the direct evaluation of the 1D spectrum for phase purity. The 2D ^{19}F CP-DARR spin diffusion experiment can detect phase mixtures by analysis of spin diffusion directly between ^{19}F nuclei.[62] The results of ^{19}F CP-DARR experiments on the 80% w/w dispersion are shown in Figure 13. The ^{19}F CP-DARR spectrum obtained with a long mixing period shows spin diffusion among the sharper peaks in the ^{19}F spectrum, which immediately indicates that these peaks arise from a single crystalline phase. The short ^{19}F T_1 of the amorphous material causes it to be filtered out with a mixing time of 160 ms, which precludes the detection of long-range spin diffusion. Because three peaks of the crystalline phase show mutual correlations in the ^{19}F CP-DARR spectrum, and given the number of fluorine atoms in **VI**, the crystalline phase in this sample is also shown to have more than one molecule in the asymmetric unit ($Z' > 1$); this is consistent with the $Z' = 2$ observed in the form III (FAFWIS02) structure. The ^{19}F CP-DARR experiment is a useful general approach to phase mixture analysis by SSNMR, in conjunction with heteronuclear-detected ^{1}H T_1 values, and may serve as a useful tool in studies of dispersions of fluorinated drug molecules.

A final experiment that deserves mention in the context of fluorinated molecules is the double-cross-polarization (DCP) experiment, involving two CP steps between ^{1}H and ^{19}F and then between ^{19}F and ^{13}C nuclei.[95] This experiment has been applied to crystalline pharmaceutical polymorphs and cocrystals.[40,80] However, it lacks the range necessary to efficiently detect interactions between ^{19}F nuclei attached to the drug and ^{13}C nuclei in the polymer in the amorphous materials of interest here because of unfavorable $T_{1\rho}$ relaxation times, and because spin diffusion does not occur during the ^{19}F−^{13}C dipolar transfers. As such, it generally requires long experiment times to detect small interactions, and lacks general utility for studies of solid dispersions. Attempts to apply long DCP experiments with various ^{19}F−^{13}C contact times on the 30% w/w dispersion of **VI** led to inconclusive results (not shown), with only intramolecular signals from **VI** itself observed clearly. However, the DCP experiment may in other cases provide detailed structural information on the interaction between fluorine atoms and the polymer for glass solutions, and thus may prove useful in some cases.

(95) Hagaman, E. W.; Burns, J. H. The determination of local structure in organofluorides using fluorine-19 carbon-13 dipolar coupling. *Fuel* **1993**, *72*, 1239–1243.

(96) Ackermann, G.; Rodloff, A. C. Drugs of the 21st century: telithromycin (HMR 3647) - the first ketolide. *J. Antimicrob. Chemother.* **2003**, *51*, 497–511.

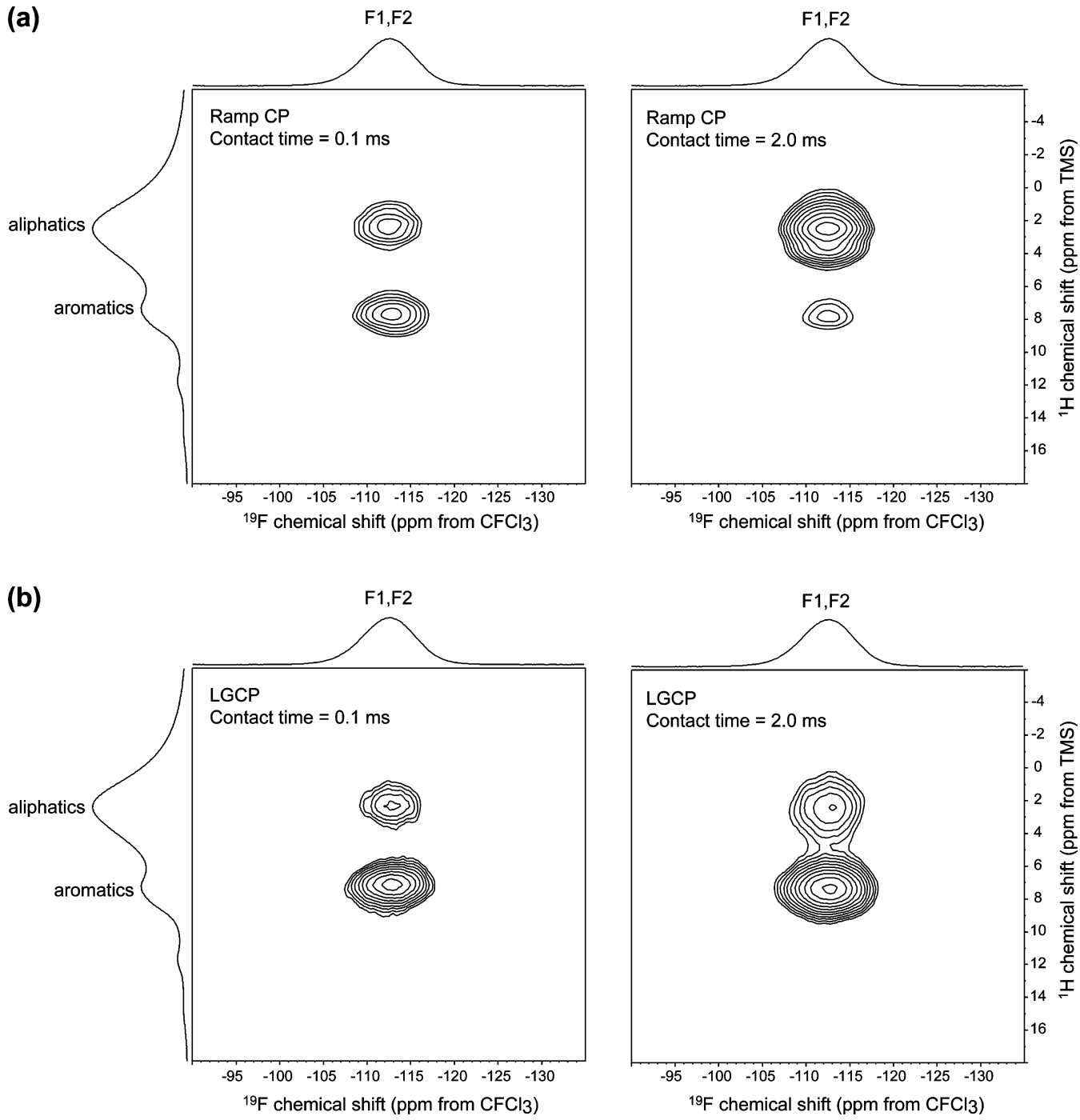

Figure 12. (a) $^{1}H-^{19}F$ CP-HETCOR spectra ($\upsilon_r = 15$ kHz) of a 30% w/w amorphous dispersion of diflunisal (**VI**) in PVP obtained with 0.1 and 2.0 ms contact times and conventional ramp CP. (b) $^{1}H-^{19}F$ LGCP-HETCOR spectra obtained under the same conditions, except with the use of LGCP to suppress spin diffusion. The difference in relative correlation intensity with a 2.0 ms contact time between the two CP methods highlights the magnitude of the spin diffusion effects between **VI** and PVP in the dispersion. The F_2 projections are the ^{19}F CP-MAS spectrum ($\upsilon_r = 15$ kHz), and the F_1 projections are the ^{1}H DP-MAS spectrum ($\upsilon_r = 35$ kHz). Spectra were obtained at 11.7 T and 273 K.

Analysis of More Complex Dispersions. To illustrate the applicability of the approaches demonstrated here to more complex scenarios, two pharmaceutical dispersions that have not been characterized in the literature were prepared. A high molecular weight drug, the antibiotic ketolide telithromycin (**VII**),[96] was chosen to show the ability of SSNMR approaches to handle larger and more complex molecules in dispersions.

The crystal structure of **VII** has not been reported in the literature. The numbering scheme shown here is a standard

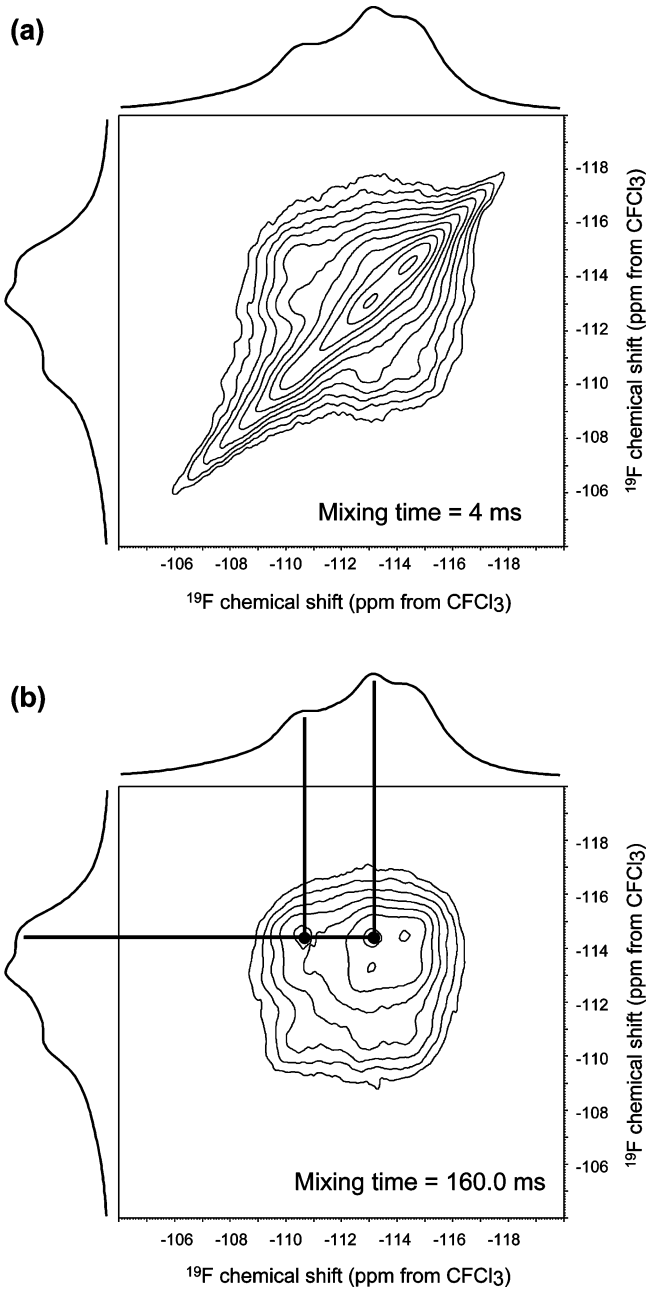

Figure 13. ^{19}F CP-DARR spectra ($\upsilon_r = 15$ kHz) of an 80% w/w amorphous dispersion of diflunisal (**VI**) in PVP at short (4 ms) and long (160 ms) mixing times, shown in (a) and (b), respectively. The F_1 and F_2 projections are the ^{19}F CP-MAS spectrum ($\upsilon_r = 15$ kHz). In (b), correlations of interest are noted between three signals that confirm these signals arise from the same phase (see text). All spectra were obtained at 11.7 T and 273 K.

scheme taken from solution-state NMR studies of **VII** and structurally related ketolides and macrolides.[97] Both crystalline and amorphous forms of **VII** have been reported.[98] The ^{13}C CP-TOSS spectrum of a 30% w/w dispersion of **VII** in PVP is compared with the input crystalline form in Figure 14(a). This dispersion showed no crystalline content by PXRD (see Supporting Information), and a single glass transition temperature of 140 °C by mDSC. The dispersion

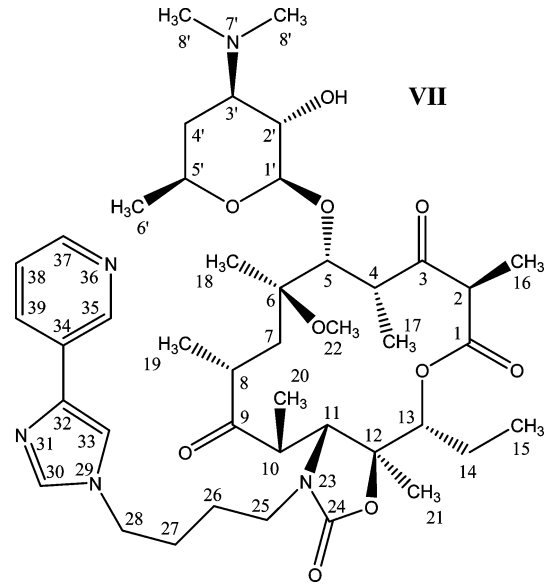

shows broad ^{13}C peaks characteristic of an amorphous phase. A ^{13}C-detected ^{1}H T_1 experiment was performed, and the signals of PVP yielded an average T_1 of 2.5 ± 0.1 s, while the T_1 of the signals of **VII** region yielded a T_1 of 2.9 ± 0.4 s (see Supporting Information). The ^{1}H T_1 values agree to within the error of the measurement, thus providing no evidence of phase separation.

The ^{1}H−^{13}C CP-HETCOR spectra of the 30% w/w dispersion of **VII** in PVP are shown in Figure 14(b). These spectra were obtained with 250 μs and 1 ms contact times. Spin diffusion effects can again be used to demonstrate the formation of a glass solution, as shown in Figure 14(b) through the increase in intensity in the shoulder correlation between the PVP carbonyl group and deshielded aromatic protons in **VII** (denoted by an arrow). Although the ^{1}H resolution is limited, comparison of the spectra obtained with short and long contact times allows for identification of the key interaction. The analysis in this case is complicated by the large number of aliphatic protons in **VII**, which cause spin diffusion to eliminate the aromatic signals entirely in the spectrum obtained with a 2 ms contact time (not shown), requiring the use of shorter 250 μs and 1 ms contact times. Drug molecules with large numbers of aliphatic protons and only a small number of aromatic protons could present a problem to the ^{1}H−^{13}C CP-HETCOR approach in some drug−polymer systems.

The final dispersion was prepared containing a fluorinated drug, a polymer, and a surfactant, and is representative of more complex products in development. Surfactants are added to amorphous dispersions to improve solubility or wettability properties beyond that obtainable with an amor-

(97) Evrard-Todeschi, N.; Gharbi-Benarous, J.; Gaillet, C.; Verdier, L.; Bertho, G.; Lang, C.; Parent, A.; Girault, J.-P. Conformations in solution and bound to bacterial ribosomes of ketolides, HMR 3647 (telithromycin) and RU 72366: A new class of highly potent antibacterials. *Bioorg. Med. Chem.* **2000**, *8*, 1579–1597.

(98) Ludescher, J.; Griesser, U.; Langes, C. Amorphous telithromycin compound. PCT Int. Appl. EP2007/000036, Nov 13, 2008.

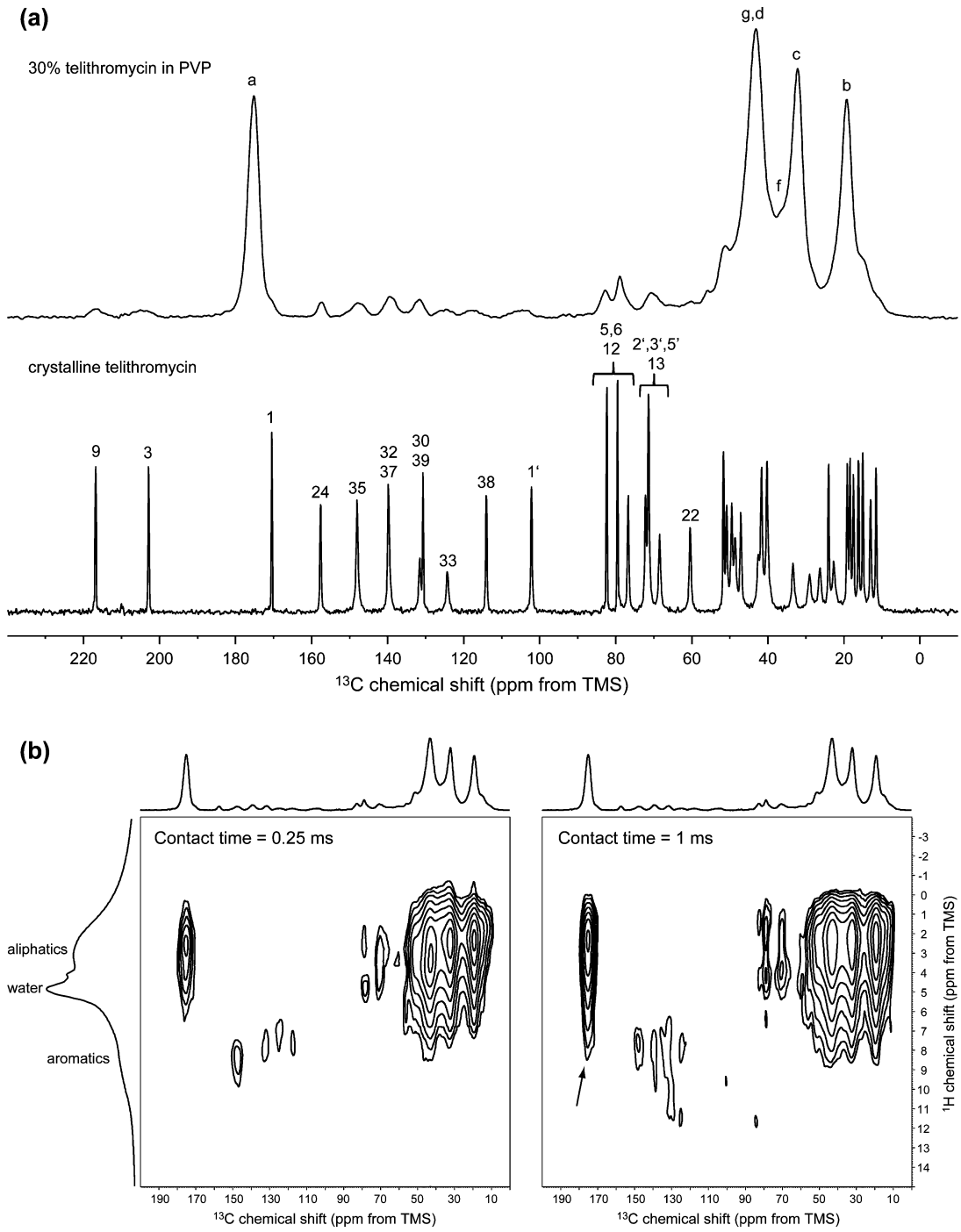

Figure 14. (a) ^{13}C CP-TOSS spectra ($\upsilon_r = 8$ kHz) of a 30% w/w amorphous dispersion of telithromycin (**VII**) compared to the crystalline input form. (b) ^{1}H−^{13}C CP-HETCOR spectra ($\upsilon_r = 12.5$ kHz) of the 30% w/w amorphous dispersion of **VII** obtained at two mixing times (250 μs and 1 ms), plotted using the same contour levels. An interaction showing spin diffusion between **VII** and PVP is denoted with an arrow. In (b), the ^{1}H MAS spectrum ($\upsilon_r = 35$ kHz) and ^{13}C CP-TOSS spectrum ($\upsilon_r = 8$ kHz) are shown as the F_1 and F_2 projections, respectively. Spectra were obtained at 9.4 T and 273 K.

phous drug/polymer system.[99−102] The drug molecule is voriconazole (**VIII**), a potent antifungal agent.[103]

The numbering scheme shown for the heavy atoms is taken from the published crystal structure of **VIII** (CSD refcode CEXMAU).[104] The hydrogen atoms are referred to here by the number of their attached heavy atom. SSNMR analysis of **VIII** has not been reported in the literature. The ^{13}C CP-TOSS spectrum of the 15% w/w dispersion of **VIII** in PVP with 5% w/w SLS is compared to the spectra of the input materials of crystalline **VIII** and SLS in Figure

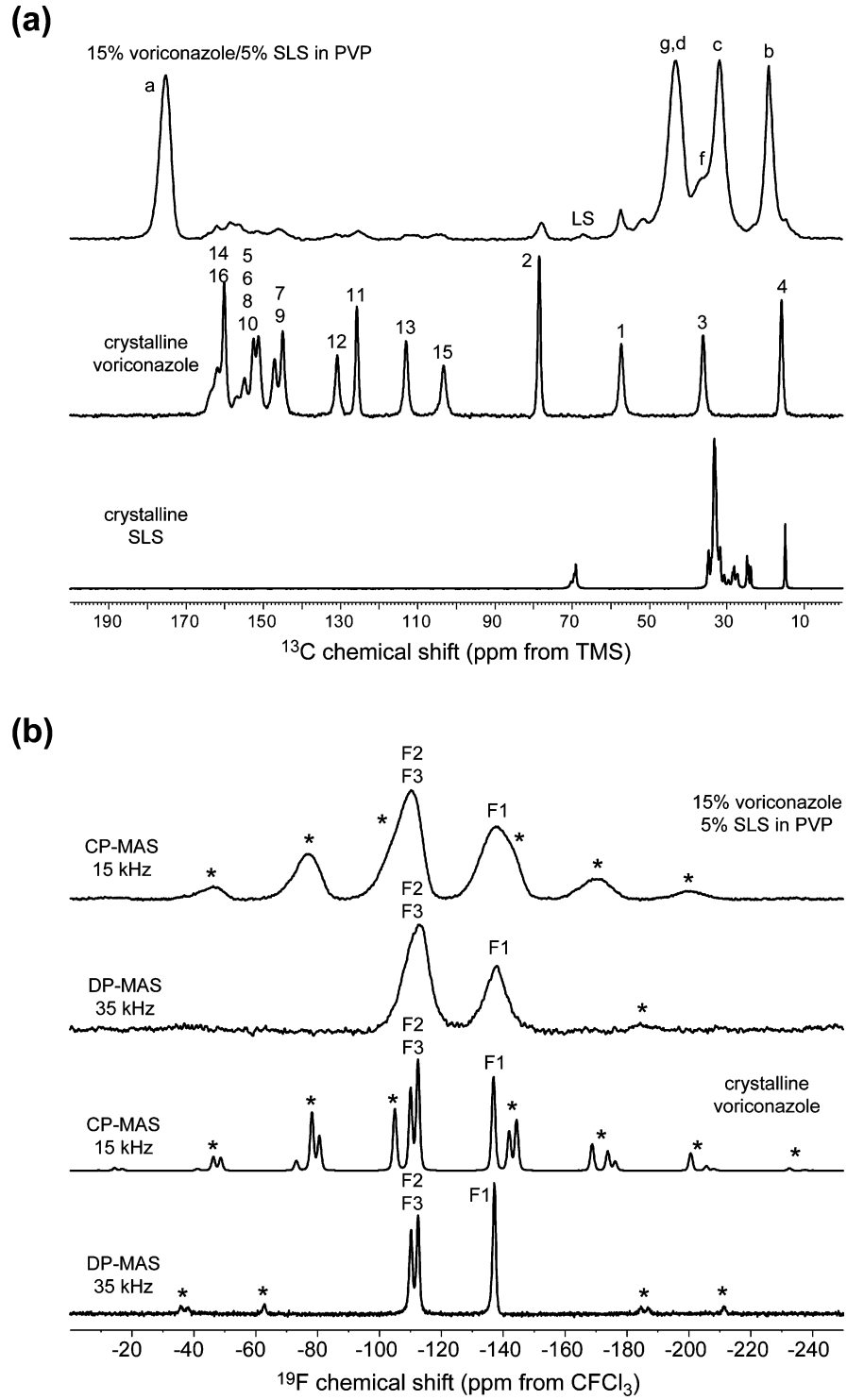

Figure 15. (a) ^{13}C CP-TOSS spectra (υ_r = 8 kHz) of a 15% w/w amorphous dispersion of voriconazole (**VIII**) in PVP with 5% w/w SLS, crystalline **VIII**, and crystalline SLS. LS denotes the signal assigned to lauryl sulfate anions in the dispersion. (b) ^{19}F CP and DP-MAS spectra of the 15% w/w amorphous dispersion of **VIII** in PVP with 5% w/w SLS obtained with the spinning rates (υ_r) shown are compared to similarly obtained spectra of crystalline **VIII**. Asterisks denote spinning sidebands. Spectra were obtained at 11.7 T and 273 K.

15(a). This dispersion showed no crystalline content by PXRD (see Supporting Information), and a single glass transition temperature of 116 °C by mDSC. The crystalline batch of **VIII** was determined to be phase-pure material of the same form as that reported in the crystal structure (see Supporting Information). The broad ^{13}C signals immediately suggest that the drug in the dispersion is amorphous. The use of dual ^{1}H and ^{19}F decoupling only

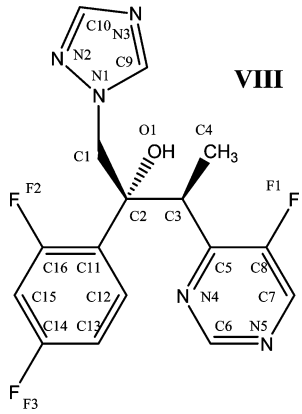

afforded minor improvements in the resolution of the **VIII** signals, as the broadening caused by disorder is more significant than that caused by dipolar broadening and *J*-coupling effects (see Supporting Information). The results of ^{19}F MAS experiments on crystalline **VIII** and the 15% w/w dispersion are shown in Figure 15(b). As **VIII** contains three fluorine atoms, the potential for overlap between spinning sidebands and centerbands exists. In these cases, fast spinning at 35 kHz provides a useful adjunct to more conventional slower-speed experiments. The ^{19}F DP-MAS spectra obtained at 35 kHz are compared to the CP-MAS spectrum obtained at 15 kHz, and allow for more straightforward assignment of the peaks using both chemical shifts and relative intensities.

Using all three accessible nuclei in the dispersion to determine ^{1}H T_1 values, as shown in Table 5, offers maximum specificity for the individual components. At υ_r = 8 kHz, the ^{13}C-detected ^{1}H T_1 values from the PVP signals yielded an average value of 6.3 ± 0.2 s. The weaker ^{13}C signals from **VIII** yielded a much poorer fit of 5.6 ± 1.4 s, because the drug is present at only 15% w/w. A more sensitive approach is to obtain ^{19}F-detected ^{1}H T_1 values for **VIII**. Using this approach, a ^{1}H T_1 of 6.3 ± 0.2 s is obtained. The ^{1}H T_1 of drug and polymer are equal within the error of the measurement, and provide no evidence of phase separation. Using ^{23}Na detection yields a T_1 of 5.8 ± 0.4 s for the sodium environment, suggesting possible phase separation. Because of N_2 ingress effects, all values reported here were obtained after ^{1}H T_1 had become constant after 5 days of equilibration time (as monitored by ^{19}F-detected ^{1}H T_1 experiments).

Table 5. ^{13}C-, ^{19}F- and ^{23}Na-Detected Chemical Shifts (δ) and ^{1}H T_1 Values of the 15% w/w Voriconazole (**VIII**) Dispersion with 5% w/w SLS, Obtained at 11.7 T, 273 K, and υ_r = 8 kHz[a]

assignment	δ (ppm)	^{1}H T_1[b] (s)
	^{13}C-Detected	
PVP (a)	172.9	6.3 ± 0.1
PVP	49.5	5.5 ± 0.6
PVP (g,d)	40.5	6.3 ± 0.1
PVP (f), 3	34.0	5.9 ± 0.2
PVP (c)	29.5	6.4 ± 0.1
PVP (b)	16.6	6.4 ± 0.1
average (PVP)		6.3 ± 0.2[c]
	^{19}F-Detected	
F_1, F_2, F_3	all peaks[d]	6.3 ± 0.2
	^{23}Na-Detected	
SLS	−10.9	5.8 ± 0.4

[a] Only the strong ^{13}C signals in the dispersion arising from PVP were fitted, as these yield the best fits for comparison with the fits from the more sensitive ^{19}F and ^{23}Na heteronuclei (see text). [b] ± estimated error from least-squares fit to the function $y = A(1 - e^{-t/T_1})$. [c] ± standard deviation from all peaks of the solid phase. [d] At υ_r = 8 kHz, the ^{19}F sideband manifold is overlapped and the entire spectrum must be integrated.

It is desirable to prove formation of a glass solution of **VIII** in PVP using only ^{1}H−^{19}F CP-HETCOR results, without recourse to lengthy ^{1}H−^{13}C CP-HETCOR experiments, which for a 15% w/w dispersion of this type would require two to three days to obtain. The ^{1}H−^{19}F CP-HETCOR spectra of the 15% w/w dispersion and form 1, obtained with increasing contact times, are compared in Figure 16. Peak intensities in ^{1}H−^{19}F CP-HETCOR spectra are influenced by spin diffusion, and as shown previously can be used to prove the formation of a glass solution. In the present case, **VIII** contains both aliphatic and aromatic proton environments that limit ^{1}H resolution. However, the presence of PVP in a glass solution contributes greatly to spin diffusion and enhancement of the intensity of correlations to aliphatic protons, so that increasing contact times in ^{1}H−^{19}F CP-HETCOR experiments (Figure 16) show that the relative increase in correlation intensity to aliphatic protons is much greater in the dispersion than in crystalline form 1. This demonstrates spin diffusion to PVP molecules in close proximity to the drug even without ^{1}H resolution. Alternatively, the ^{1}H−^{19}F CP-HETCOR

(99) de Waard, H.; Hinrichs, W. L. J.; Visser, M. R.; Bologna, C.; Frijlink, H. W. Unexpected differences in dissolution behavior of tablets prepared from solid dispersions with a surfactant physically mixed or incorporated. *Int. J. Pharm.* **2008**, *349*, 66–73.

(100) Morris, K. R.; Knipp, G. T.; Serajuddin, A. T. M. Structural properties of polyethylene glycol - polysorbate 80 mixture, a solid dispersion vehicle. *J. Pharm. Sci.* **1992**, *81*, 1185–1188.

(101) Mura, P.; Moyano, J. R.; Gonzalez-Rodriguez, M. L.; Rabasco-Alvarez, A. M.; Cirri, M.; Maestrelli, F. Characterization and dissolution properties of ketoprofen in binary and ternary solid dispersions with polyethylene glycol and surfactants. *Drug Dev. Ind. Pharm.* **2005**, *31*, 425–434.

(102) Ghebremeskel, A. N.; Vemavarapu, C.; Lodaya, M. Use of surfactants as plasticizers in preparing solid dispersions of poorly soluble API: Selection of polymer-surfactant combinations using solubility parameters and testing the processability. *Int. J. Pharm.* **2007**, *328*, 119–129.

(103) Dickinson, R. P.; Bell, A. S.; Hitchcock, S.; Narayanaswami, S.; Richardson, K.; Troke, P. F. Novel antifungal 2-aryl-1-(1*H*-1,2,4-triazol-1-yl) butan-2-ol derivates with high activity against *Aspergillus fumigatus*. *Bioorg. Med. Chem. Lett.* **1996**, *16*, 2031–2036.

(104) Ravikumar, K.; Sridhar, B.; Prasad, K. D.; Rao, A. K. S. B. Voriconazole, an antifungal drug. *Acta Crystallogr.* **2007**, *63*, o565−o567.

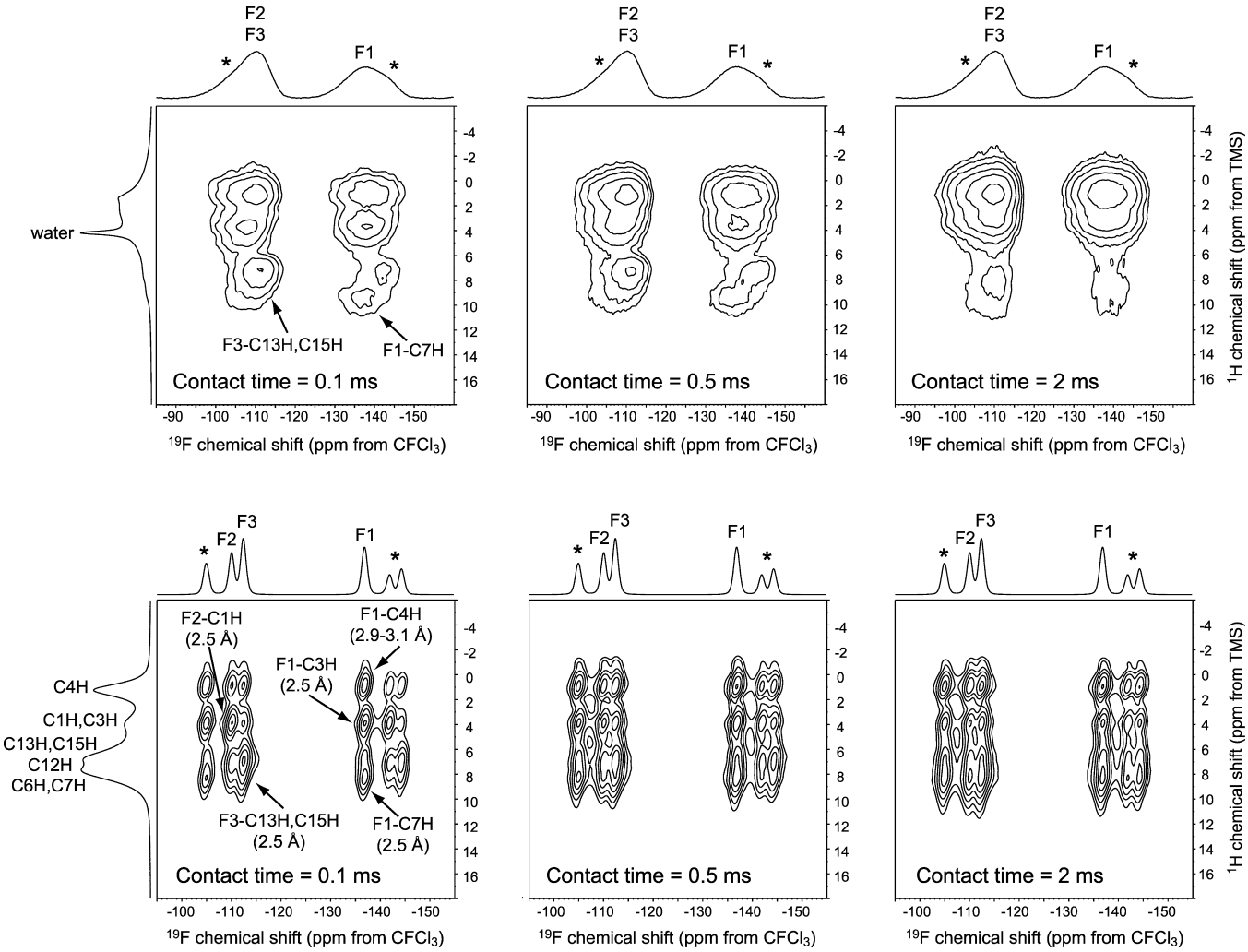

Figure 16. (a) ^{1}H−^{19}F CP-HETCOR spectra (υ_r = 15 kHz) of the 15% w/w amorphous dispersion of voriconazole (**VIII**) in PVP with 5% w/w sodium lauryl sulfate obtained with different mixing times. (b) ^{1}H−^{19}F CP-HETCOR spectra of crystalline **VIII** obtained under the same conditions. The distances shown in (b) are taken from the crystal structure (ref 104). The F_2 projections are ^{1}H spectra (υ_r = 35 kHz), while the F_2 projections are ^{19}F CP-MAS spectra (υ_r = 15 kHz). All spectra were obtained at 11.7 T and 273 K.

spectrum of the dispersion with a 2 ms contact time can be compared to the ^{1}H−^{19}F LGCP-HETCOR spectrum obtained with the same contact time (see Supporting Information); the lack of spin diffusion during LGCP leads to an equal distribution of aliphatic−aromatic correlation intensity. The main advantage of the ^{1}H−^{19}F LGCP-HETCOR spectrum is that it can be used for comparison with the ^{1}H−^{19}F CP-HETCOR spectrum to determine if spin diffusion to PVP occurs without the need for a separate sample of the drug.

The physical state of SLS appears amorphous from the PXRD pattern and the ^{13}C CP-TOSS spectrum, the latter evidenced by a broad peak in Figure 15 (marked "LS") at 67 ppm. An orthogonal view of the SLS environment is provided by ^{23}Na SSNMR. The sodium is likely in close proximity with the lauryl sulfate anion (LS), as PVP is nonionic and **VIII** is not likely to form base-addition salts. Besides the evidence of phase separation between SLS and the glass solution of PVP and **VIII** provided by the multinuclear ^{1}H T_1 measurements described above, the ^{1}H−^{23}Na CP-HETCOR experiment can also be used to scout for potential spin diffusion involving the sodium site. The ^{1}H−^{23}Na CP-HETCOR spectra obtained at short and long contact times are shown in Figure 17 and show no evidence of spin diffusion to aromatic protons on **VIII** or aliphatic protons on PVP; instead, a moderate intensity increase is observed with spin diffusion effects shifting the correlation to more shielded ^{1}H frequencies, suggesting diffusion along the LS chain to the terminal methyl group, which has the most shielded resonance of any peak in SLS, **VIII**, or PVP. This result agrees with the phase separation detected by the ^{23}Na-detected ^{1}H T_1 experiment.

Although the ^{23}Na CP-MAS and DP-MAS spectra of the dispersion are broad and structureless, the MQ-MAS experiment with triple-quantum excitation can be utilized to help uncover structure obscured by second-order quadrupolar broadening.[64] The sheared MQ-MAS spectrum of the dispersion is given in Figure 18(a) and shows at least three peaks in the isotropic dimension, suggesting multiple sodium environments and a complex structure for the surfactant

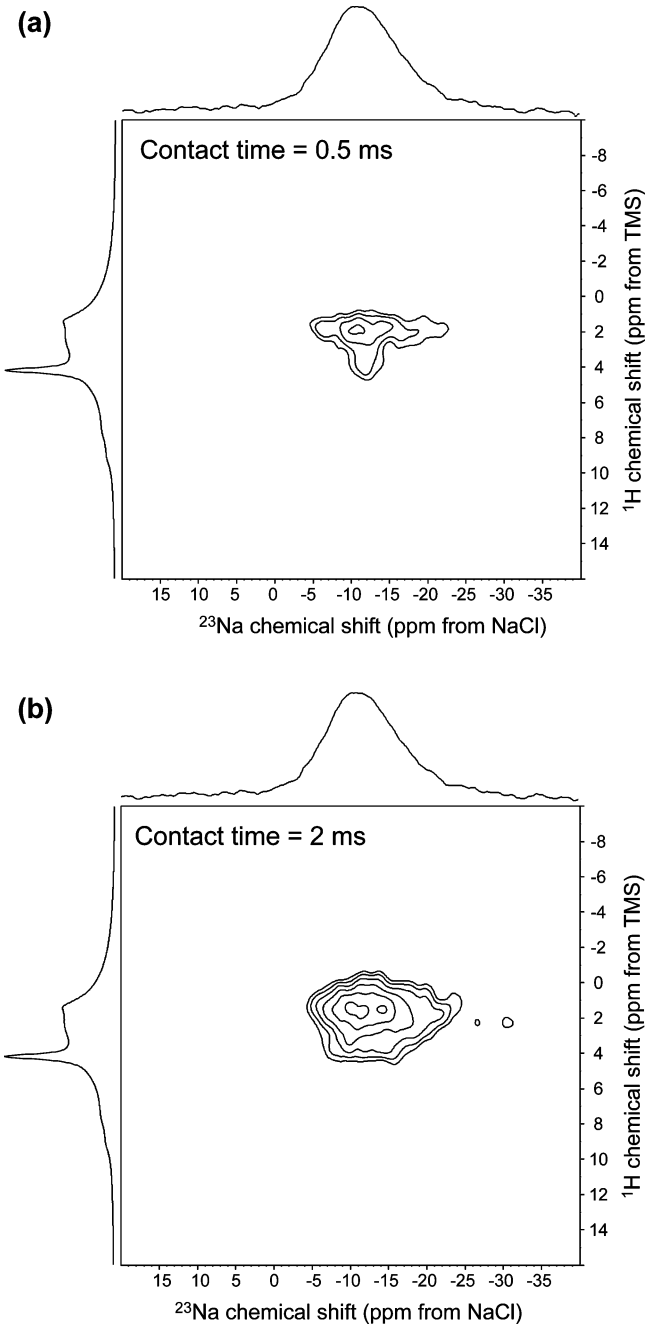

Figure 17. ^{1}H−^{23}Na CP-HETCOR spectra (υ_r = 15 kHz) of the 15% w/w amorphous dispersion of voriconazole (**VIII**) in PVP with 5% w/w SLS obtained with a 500 μs (a) and 2 ms (b) contact time. The ^{23}Na CP-MAS spectrum (υ_r = 15 kHz) and ^{1}H DP-MAS spectrum (υ_r = 35 kHz) are shown as projections. The same contour levels were used to plot each spectrum. All spectra were obtained at 11.7 T and 273 K.

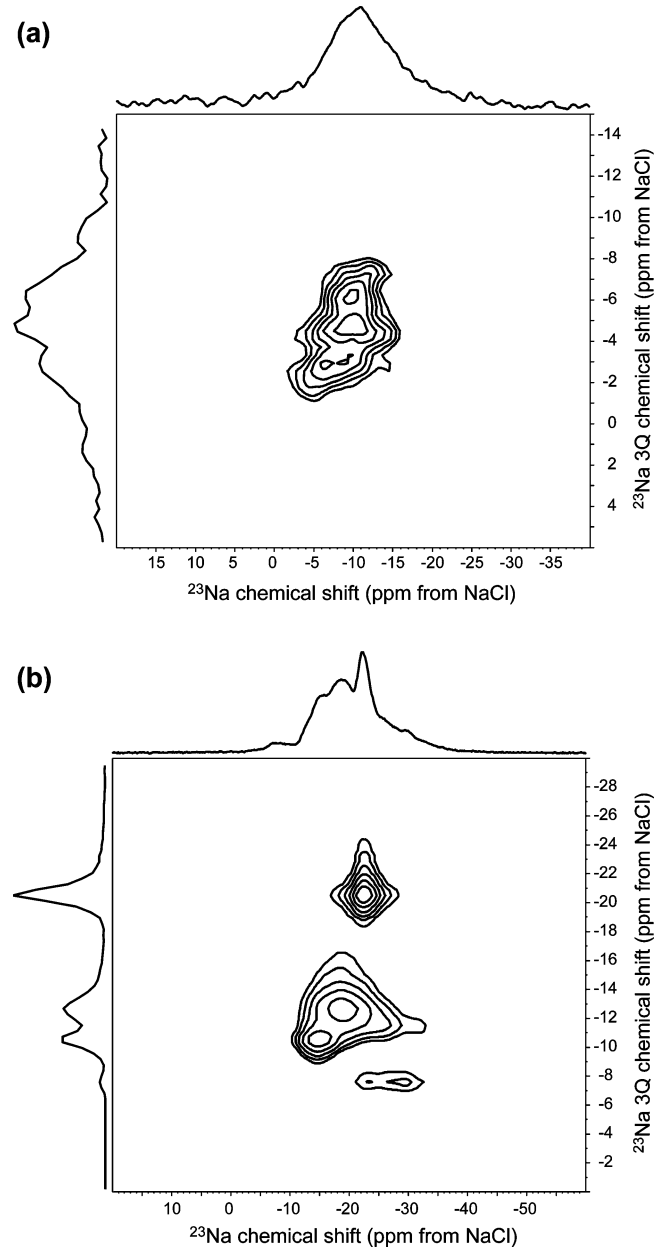

Figure 18. ^{23}Na MQ-MAS spectrum (υ_r = 25 kHz) of the 15% w/w amorphous dispersion of voriconazole (**VIII**) in PVP with 5% w/w SLS (a), compared to the MQ-MAS spectrum of the input SLS batch (b). The F_1 projections shown are skyline projections along the sheared triple-quantum dimension, and the F_2 dimension projections are the ^{23}Na DP-MAS spectra (υ_r = 25 kHz). Spectra were obtained at 11.7 T and 273 K.

within this material. The sodium environment in the dispersion is more deshielded than the major sites in a typical sample of crystalline SLS, as seen in Figure 18(b), indicating that the sodium is more hydrated in the dispersion, as increasing water content in polymer matrices is known to lead to deshielding trends on ^{23}Na chemical shifts.[105] Further investigations of ^{23}Na environments in such dispersions are planned to determine the utility of SSNMR in the investigation of batch-to-batch variation in SLS-containing dispersions.

Conclusions

In this study, 2D SSNMR dipolar correlation methods and ^{1}H T_1 relaxation measurements have been shown to be a powerful tool for structural analysis of amorphous solid dispersions. These structural methods augment previously demonstrated SSNMR methods for analysis of molecular

mobility in dispersions.[42−45] The structural analysis methods explored in this work have been found to be particularly useful for the identification of the presence of glass solutions from a single sample without the need for preparation or analysis of reference materials. Heteronuclear-detected ^{1}H T_1 measurements were found to provide straightforward detection of phase separation in amorphous dispersions. Several different methods for directly proving glass solution formation were demonstrated in this work. The $^{1}H-^{13}C$ CP-HETCOR experiment performed with a long contact time relies on spin diffusion between the drug and the polymer in glass solutions; the ^{1}H chemical shift resolution is sufficient because most polymers used to form dispersions do not contain aromatic groups. This approach to confirming glass solution formation has the important advantage of not requiring the preparation of amorphous reference material and/or physical mixtures for comparison, although this can be done if desired (as shown for indomethacin). The more sensitive $^{1}H-^{19}F$ CP-HETCOR experiment can readily detect spin diffusion between fluorinated drug molecules and polymers in glass solutions. Another useful approach demonstrated in this work is the evaluation of gross signal intensity variations caused by spin diffusion to proton-rich polymers, which can prove glass solution formation even in the absence of adequate ^{1}H resolution. Finally, a range of other SSNMR experiments, including the ^{1}H DQ-BABA, ^{2}H, and ^{23}Na experiments, have been shown to play a useful supporting role in the analysis of dispersions. The present work has demonstrated that SSNMR can handle more complex dispersions than DSC and PXRD and obtain more definitive structural information with less data analysis and interpretation. Finally, it should be noted that a number of SSNMR experiments were not utilized in the present work but further improve the analysis of amorphous pharmaceutical dispersions. For example, T_1 and $T_{1\rho}$ measurements as a function of temperature can characterize molecular mobility in dispersions.[44,45] Combined application of these techniques should allow for insight into critical questions about the physical and chemical stability of dispersions, and the impact of water on recrystallization, through correlations between structure, relaxation times, and mobility in the solid state.[14,15,42,43]

Supporting Information Available: Additional PXRD data and SSNMR spectra for the materials used in this study. This material is available free of charge via the Internet at http://pubs.acs.org.

MP100205G

(105) Wang, P.; Ando, I. Structural characterization of hydrated poly(aspartic acid) sodium and poly(aspartic acid) sodium/poly(vinyl alcohol) blends by high-resolution solid-state ^{23}Na NMR. *J. Mol. Struct.* **1999**, *508*, 97–102.